UNIVERSIDADE ESTADUAL DE CAMPINAS
Faculdade de Engenharia Elétrica e de Computação

Adelson Duarte dos Santos

Electronic Sensors for Grain Storage: A Reconfigurable Multisensor Design based on PCB Technology

Sensores para armazenamento de grãos: design de multisensor reconfigurável baseado em PCB

Campinas

2023

Adelson Duarte dos Santos

Electronic Sensors for Grain Storage: A Reconfigurable Multisensor Design based on PCB Technology

Sensores para armazenamento de grãos: design de multisensor reconfigurável baseado em PCB

Thesis presented to the School of Electrical and Computer Engineering in partial fulfilment of the requirements for the degree of Doctor in Electrical Engineering, in the area of Electronics, Microelectronics and Optoelectronics.

Tese apresentada à Faculdade de Engenharia Elétrica e de Computação como parte dos requisitos exigidos para a obtenção do título de Doutor em Engenharia Elétrica, na Área de Eletrônica, Microeletrônica e Optoeletrônica.

Supervisor: Prof. Dr. José Antonio Siqueira Dias

Co-supervisor Prof. Dr. Elnatan Chagas Ferreira

Este trabalho corresponde à versão final da tese defendida pelo aluno Adelson Duarte dos Santos, e orientado pelo Prof. Dr. José Antonio Siqueira Dias.

Campinas

2023

Ficha catalográfica
Universidade Estadual de Campinas
Biblioteca da Área de Engenharia e Arquitetura
Rose Meire da Silva - CRB 8/5974

Santos, Adelson Duarte dos, 1992-
Sa59e Electronic sensors for grain storage : a reconfigurable multisensor design based on PCB technology / Adelson Duarte dos Santos. – Campinas, SP : [s.n.], 2023.

Orientador: José Antonio Siqueira Dias.
Coorientador: Elnatan Chagas Ferreira.
Tese (doutorado) – Universidade Estadual de Campinas, Faculdade de Engenharia Elétrica e de Computação.

1. Multisensores. 2. PCB. 3. Grãos - Armazenamento. 4. Medidores de umidade. 5. Medição de temperatura. I. Dias, José Antonio Siqueira, 1954-. II. Ferreira, Elnatan Chagas, 1955-. III. Universidade Estadual de Campinas. Faculdade de Engenharia Elétrica e de Computação. IV. Título.

Informações Complementares

Título em outro idioma: Sensores para armazenamento de grãos : design de multisensor reconfigurável baseado em PCB
Palavras-chave em inglês:
Multisensor
PCB based sensors
Grain storage
Moisture sensors
Temperature sensors
Área de concentração: Eletrônica, Microeletrônica e Optoeletrônica
Titulação: Doutor em Engenharia Elétrica
Banca examinadora:
José Antonio Siqueira Dias [Orientador]
Anderson Wedderhoff Spengler
Luís Fernando Caparroz Duarte
José Alexandre Diniz
Flávio José de Oliveira Morais
Data de defesa: 25-09-2023
Programa de Pós-Graduação: Engenharia Elétrica

Identificação e informações acadêmicas do(a) aluno(a)
- ORCID do autor: https://orcid.org/0000-0001-8396-1760
- Currículo Lattes do autor: http://lattes.cnpq.br/4140425884455749

COMISSÃO JULGADORA - TESE DE DOUTORADO

Candidato(a): Adelson Duarte dos Santos RA: 190710
Data de defesa: 25 de Setembro de 2023
Título da Tese: "Electronic Sensors for Grain Storage: A Reconfigurable Multisensor Design based on PCB Technology"

Prof. Dr. José Antonio Siqueira Dias (Presidente)
Prof. Dr. Flávio José de Oliveira Morais
Prof. Dr. Luís Fernando Caparroz Duarte
Prof. Dr. Anderson Wedderhoff Spengler
Prof. Dr. José Alexandre Diniz

A Ata de Defesa, com as respectivas assinaturas dos membros da Comissão Julgadora, encontra-se no SIGA (Sistema de Fluxo de Dissertação/Tese) e na Secretaria de Pós-Graduação da Faculdade de Engenharia Elétrica e de Computação.

À todas as pessoas de coragem, amor e paciência que habitaram a América do Sul.

Acknowledgements

This work is the end result of many thoughts and experiences that I have had contact with over these four years. Several notable people I would like to express my gratitude to:

My advisor, Prof. Dr. José Antonio Siqueira Dias, for his vast knowledge in electronics and scientific method. Also thanks for his patience and encouragement during this hard time in Brazilian science. I am delighted to have deeply learned electronics and related topics under his supervision. To the National Council for Scientific and Technological Development (CNPq), for supporting this thesis in the best feasible way.

Prof. Dr. Robert Neal Dean, from Auburn University. Prof. Robert Neal Dean was highly receptive to collaboration in this research. Although Prof. Robert invited me as a visiting PHD student, the social and personal conjuncture of the period 2019-2023 in which I experienced did not make this experience possible.

Flávio Morais, a colleague who supported me technically and guided me at the beginning of this journey. Since my master's degree, Prof. Flávio Morais has been in the surroundings, so thank you very much for your kindness.

My colleague from the now extinguished department of electronics and microelectronics (DEMIC), Prof. Dr. Rodrigo Moreira Bacurau, whose resilience and humbleness are admirable.

Dr. Marcelo Vinicius de Paula, Mathias Scroccaro and Marllon Schlischting, whose social context we shared during a portion of the time of this work. Also colleagues from department of electronics and biomedical engineering: Heitor Fernandes and Dra. Debora Matoso.

Especially to the Lobo Family, with emphasis on the uniqueness of the social scientist and philosopher Jéssica Gonçalves Lobo, who walked this long road with me and certainly provided important learning during this period.

Particularly to mother nature, that provides everything for us all.

Finally, I would like to congratulate myself, for having managed to endure all the adversities of this period. As wekk as having maintained focus, discipline and hope in the face of a shattered reality.

"A engenharia cai sobre as pedras
Um curupira já tem o seu tênis importado
Não conseguimos acompanhar o motor da história
Mas somos batizados pelo batuque e apreciamos a agricultura celeste.
Mas enquanto o mundo explode
Nós dormimos no silêncio do bairro
Fechando os olhos e mordendo os lábios
Sinto vontade de fazer muita coisa."
(Chico Science & Nação Zumbi)

Resumo

Nesta tese, apresentamos contribuições relacionadas a circuitos eletrônicos e sensores ambientais reconfiguráveis. Apresentamos o projeto de um multisensor reconfigurável baseado na tecnologia PCB para medir a temperatura e o teor de umidade de grãos. A partir dos processos de confecção de PCBs, é possível implementar sensores e seus circuitos de condicionamento de maneira integrada, dedicados a fornecer medidas ambientais em tempo real dentro da infraestrutura de armazenamento de grãos. Na área de design de sensores, apresentamos uma valiosa contribuição. A nova estrutura de multisensores é composta por trilhas de cobre dispostas de forma paralela ao longo de uma simples PCB FR-4, formando um capacitor de efeito de franja (*fringing field capacitor*), o qual linhas de campo elétrico são formados não paralelamente as placas condutivas. Além disso, pode-se usar as trilhas de cobre como sensores de temperatura. A reconfiguração da estrutura de detecção permite a compensação adequada da variação da capacitância em função da temperatura, além de permitir a integração de sensores no mesmo substrato. Na área de design de circuitos, apresentamos o primeiro sensor reconfigurável baseado na tecnologia PCB para medições de temperatura e teor de umidade aplicado a material sólido e organico. O circuito de medição de temperatura foi projetado a partir da modificação da ponte de Wheatstone, a qual trouxe acréscimos significativos na linearidade e na calibração. O sensor com eletrodos de cobre desenvolvido apresentou uma sensibilidade de $21.07\,\mathrm{m\Omega/^{\circ}C}$ na faixa de $10\,^{\circ}\mathrm{C} \leq \mathrm{T} \leq 50\,^{\circ}\mathrm{C}$ e erro de $\mid E_{nl} \mid = 0.64\,^{\circ}\mathrm{C}$ quando polarizado por uma corrente de 10 mA. A leitura da umidade foi realizada pelo efeito capacitivo, em conjunto com a técnica de intervalo de tempo e conversão frequência-tensão. A capacitância do sensor apresentou sensibilidade de $0.98\,\%/\mathrm{pF}$ e variação de $\Delta C = 14.6\,\mathrm{pF}$ na faixa de umidade de 9 % to 27 % para grãos de milho. Além disso, as medições de umidade apresentaram desvio padrão menor (1 pF part 257 pF) do que o estado da arte disponível atualmente (1 pF part 90 pF), ao considerar diferentes arranjos de grãos de milho sobre o sensor.

Palavras-chaves: Multisensores; PCB; Grãos - armazenamento; Medidores de umidade; Medição de temperatura.

Abstract

In this thesis, we present contributions regarding circuits and components for reconfigurable multisensors and smart environmental sensors. We introduce a smart multisensor design based on PCB technology to measure temperature and moisture content which extends the potential monitoring of stored grain. By leveraging the PCB design and fabrication process, it is possible to deploy application-specific sensors to provide real-time measurements within the grain storage infrastructure. The valuable contribution presented is that the novel multisensing structure is comprised of copper tracks arranged in parallel along an ordinary FR-4 PCB creating a fringing field capacitor. Additionally, the copper tracks can also operates as a resistive temperature detector. These reconfigurable characteristics of the sensing structure allow proper compensation for the variation of fringing field capacitance, as well as allowing sensors to be integrated into the same substrate. The first reconfigurable smart sensor based on PCB technology for measuring temperature and moisture content of solid and organic materials has been presented. The temperature measurement circuit was developed by modifying the Wheatstone bridge, which led to improvements in linearity and calibration. The fabricated sensing element provided a sensitivity of 21.07 mΩ/°C in the range of 10 °C $\leq$ T $\leq$ 50 °C, and an error of $\mid E_{nl} \mid = 0.64$ °C when driven by 10 mA. Moisture measurements were designed using the time-interval technique and a frequency-to-voltage conversion. The proposed fringing field capacitance showed sensitivity of 0.98 %/pF and a $\Delta C = 14.6$ pF using corn kernels with a moisture content range of 9 % to 27 %. Also, the moisture measurements presented a smaller standard deviation (1 pF part 257 pF) compared to the current available state-of-the-art measurement (1 pF part 90 pF) when considering different arrangements of corn kernels over the sensor.

Keywords: Multisensor; PCB based sensors; Grain storage; Moisture sensors; Temperature sensors;

List of Figures

List of Tables

Contents

1 Introduction

We started the second decade of the twenty-first century facing the increasing food security issues due to the instability within global value chains caused by the COVID-19 pandemic and a war situation involving two key world exporters of grains and oilseeds. The projections from this scenario suggest that food consumption will not increase sufficiently to meet the sustainable development goal 2 on Zero Hunger by 2030 [1].

In our local scenario, Brazil is facing a record grain production in 2023 also oriented towards increasing yields using the same amount of land. This approach seems to be the appropriate, since we hope to slow down or even stabilize the rate of agricultural land use and instead protect and recover our natural biome. The agricultural production record in the country over the last 20 years, largely guided by soybeans, the sugar-alcohol complex, meat, forestry products, coffee and grains, flours and preparations, which accounted for 86% of exports in 2021, has generated a succession of positive balances in the national account. The Fig. 1.1 shows Brazil's agribusiness trade balance from 2000 to 2021 based on the data of The Brazilian Agricultural Research Corporation (Embrapa) [2].

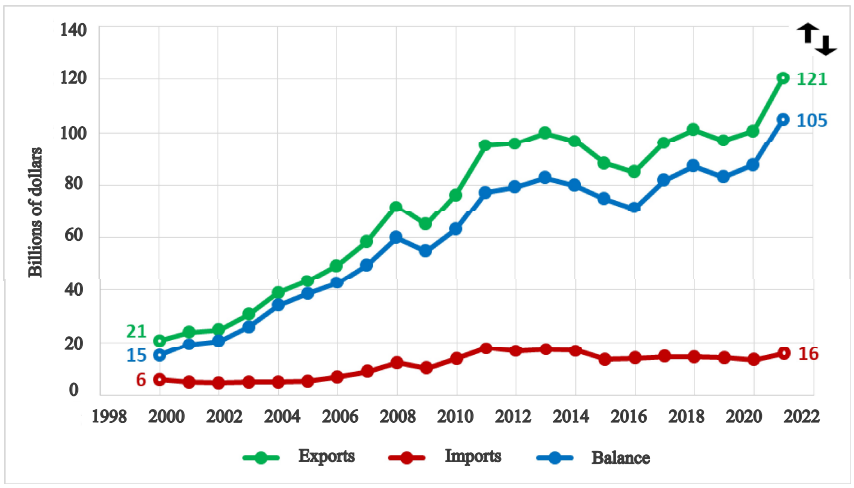

Figure 1.1 – Brazil's agribusiness trade balance from 2000 to 2021

Agricultural production involves the transformation of natural resources into goods for our society [3]. It requires a multidisciplinary approach to efficiently optimize this process through natural resource management, culture-specific and spatial location expertise, and technological solutions. The sustainable development agenda (also known as 2030 Agenda) was set up in 2015 by United Nations General Assembly (UN-GA) in order to address new agriculture approaches to provide sustainable food production systems and resilient agricultural practices [3].

Post-harvest losses can represent around one-quarter of the consumed water, cropland and fertilize used to produce food [4]. A share of the losses can be traced back to insufficient infrastructure for grain storage. These facilities are widely found in low/middle income countries (including Brazil), where there is a lack of investment in technologies for storage systems. The poor environmental conditions lead to grain deterioration due to high temperatures; mould development or pest infestation stems from the uncontrolled humidity [5, 6].

Healthy grains can be stored for long periods when there is a monitoring and controlling system within the storage environment to ensure an adequate range of grain temperature and moisture content during different external weather conditions. One solution is an aeration system to control the environment within the storage infrastructure using a controlled air circulation [6]. To contribute to the optimization of the aeration process, a study of environmental sensing elements is proposed.

This thesis presents a contribution in environmental multisensors based on printed circuit board technology (PCB) applied to precision agriculture. The integration of the proposed multisensing may enable on site precision measurement of the environmental, thus providing valuable data for post data processing, by data fusion algorithms. This chapter is divided into three parts: the first one deals with environmental sensors, the second part is dedicated to multisensors measurement systems, and the final section focuses on printed circuits.

1.1 Environmental sensors

Environmental monitoring is required to protect live organisms from toxic contaminants and pathogens that can be released into a variety of media including air, soil, and water [7]. These systems make use of data provided by temperature sensors, gases, humidity, pH, among others [8], which reveal details about these media of different kinds. Also these sensors can operate within controlling systems, optimizing the amount of natural resources applied in different industries, including agriculture.

Precision agriculture is a branch of sustainable agricultural practices that uses high-tech systems through the internet of things, artificial inteligence, and sensor technology to collect, process, and then analyze temporal, spatial, and individual data, fusing them to support management decisions geared towards increasing crop yields while mitigating natural resource inputs. [9, 10]. In this thesis, we investigate a novel multisensing architecture consisting of resistance temperature detector (RTD) and capacitive fringe field sensors integrated on a glass-reinforced epoxy laminated material (FR-4) substrate using the printed circuit board technology. We focused our work on temperature and moisture content measurement systems, which play a key role in environmental monitoring.

1.2 Multisensor measurement systems

Multisensing measurement systems are those that employ multiple sensors to provide a path for in-depth information in a given process. These systems are becoming widespread in modern industrial applications, in which data fusion driven solutions and massive deployment of the internet of things may facilitate the flow of information from raw data to a high-level of understanding and insights [11, 12].

Data fusion algorithms are the key signal processing technique to get comprehensive information from complex industrial multisensing systems. There are numerous different methods to fusion multisensing throughput [12]. Therefore, an integrated environmental multi-sensor system in addition to data fusion techniques can enhance the reliability and robustness of data acquisition in the field.

Although a comprehensive understanding of data fusion and its processing techniques is beyond the scope of this work; to whom this issue may interest, there are studies that discuss data fusion in precision agriculture [10, 13, 14, 15].

1.3 Printed circuits

Printed circuits consist of a thin coat of electrically conductive material applied to a pattern on an insulating substrate [16]. The introduction of this type of circuit at the beginning of the second half of the twentieth century allowed the advances in the manufacturing of electronic equipment, reducing their size, weight and improving reliability.

FR-4 is the most commonly used base material for PCB due to its electrical, mechanical, and thermal properties, that suit for a wide range of applications. This is fundamentally a base material made up of a composition of resin, reinforcement and the conductive foil, acting as an essential building block of printed circuits, and therefore, the basis of electronic equipments [17].

Printed sensors can also exploit the use of the standard materials and fabrication process for low-cost commercial PCB. In this work, these sensors are custom-designed by a copper (Cu) electrode pattern on FR-4 substrate that can interact with the near surrounding. It seems to be an interesting solution for low-cost environmental sensors in precision agriculture pwing to they straightforward design process.

2 Literature review

This chapter presents the literature review of moisture content sensors, temperature sensors and environment multisensors .

2.1 Moisture content sensors

Moisture sensors are employed whenever it is desirable to measure the volumetric water content of a solid material and they are widely found in agricultural applications. Soil moisture measurement can be used to determine the operation of the irrigation system on a farm or the best moment for harvesting [18]. Also, moisture sensors can be applied to assist the monitoring of food stocks [19]. Any biological activity requires a good relation between temperature and moisture - liquid water content in a solid - or humidity - water vapor concentration in a gas. Therefore, It is evident that moisture sensors play a key role in environmental science. Some techniques for acquiring this information are briefly described below.

2.1.1 Grain moisture content sensing methods

There is no homogeneity in granular samples. Physical properties, such as grain shape, and chemical properties can directly influence the measurement. Several techniques have been proposed in order to improve this accuracy. However, this improvement may be associated with disadvantages such as poor agility and destruction of the monitored sample. The techniques used can be divided into direct and indirect measurement techniques.

2.1.2 Direct methods

Direct measurement techniques are based on the dehydration of a sample through exposure to a heat source or a selective chemical reaction. The international guideline for moisture content determination is established by first exposing a 8-35 g sample for 38 hours at a temperature of 130 °C over 3 sessions [20]. After that the sample is cooled for 30 - 45 minutes. Through the use of an oven and the subsequent gravimetric analysis, it is possible to predict the volatilized weight and consequently the initial moisture content of the collected sample.

Since the sample is under severe stress from long exposure times at elevated temperatures, it can often lead to the destruction of the analyzed sample. The slow dynamics of this technique also creates prolonged waiting for results. Many labor hours are dedicated to gathering the moisture of the sample, and any mistakes could further

increase the time it takes to collect the results, thus making it a costly technique in terms of time and effort.

Conversely, the direct measurement approaches are very reliable thanks to their internationally acknowledged and yield lowest measurement uncertainty among all available methods.

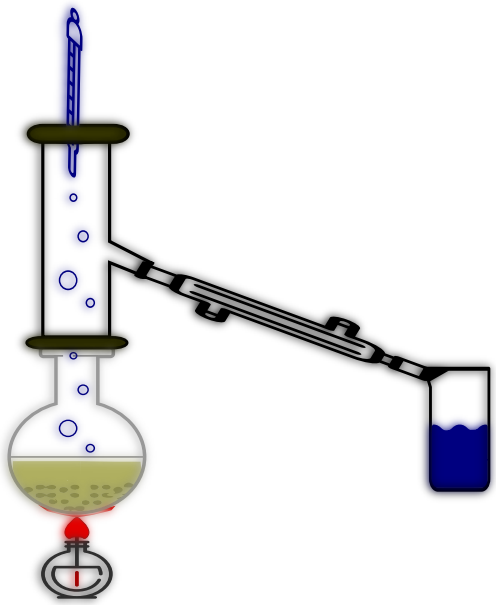

Figure 2.1 – Distillation process for moisture content measurement.

Similar to the previous method, the distillation also employs a heat source as a catalyst in the process of removing water from the sample [21]. The source of heat is attached to a distillation flask, which is connected to a condenser in the upper part, and the resultant liquid is fed into a graduated glass vial, as shown in Fig. 2.1.

In this scenario, the kernels are immersed into oil and the boiling of the most volatile element of the mixture - in this case water - is accelerated by heat. The vapor is condensed and then transferred to a graduated tube. Thus it is possible to obtain the amount of water present in the grain sample. The main disadvantage of this method is the damage to the analyzed sample.

Finally, the Karl Fischer titration technique [22], widely used for the determination of water concentration in different products and contexts, such as biological samples and chemical products, can also be used for granular materials. This technique is based on the addition of specific solvents and reagents to the grain sample, which electrochemically interact with the water, leading to a current proportional to the amount of water in the sample. This technique is fast and environmentally uncontaminated. Nevertheless, the analyzed sample is destroyed.

2.1.3 Indirect methods

Indirect methods are those that offer more feasibility and speed of sample moisture measurement [20]. As opposed to the previous method, it can be used to carry out in situ measurement quickly without destroying the sample. Such advantages encourage real-time integration of monitoring systems with decision-making algorithms based on the gathered data.

Being aware of the constraints of the method, one can add compensating techniques to reduce the measurement uncertainty, such as measuring humidity and temperature with the same sensor [23].

The technique of electrical resistance is shown in Fig. 2.2. It primarily involves measuring the electrical resistance between two electrodes whose constant current passes through the grain (located between these electrodes). The wetter the grain is, the lower the electrical resistance of the sample will be. It is obtained a curve in which the resistance increases as the moisture value decreases [20, 24].

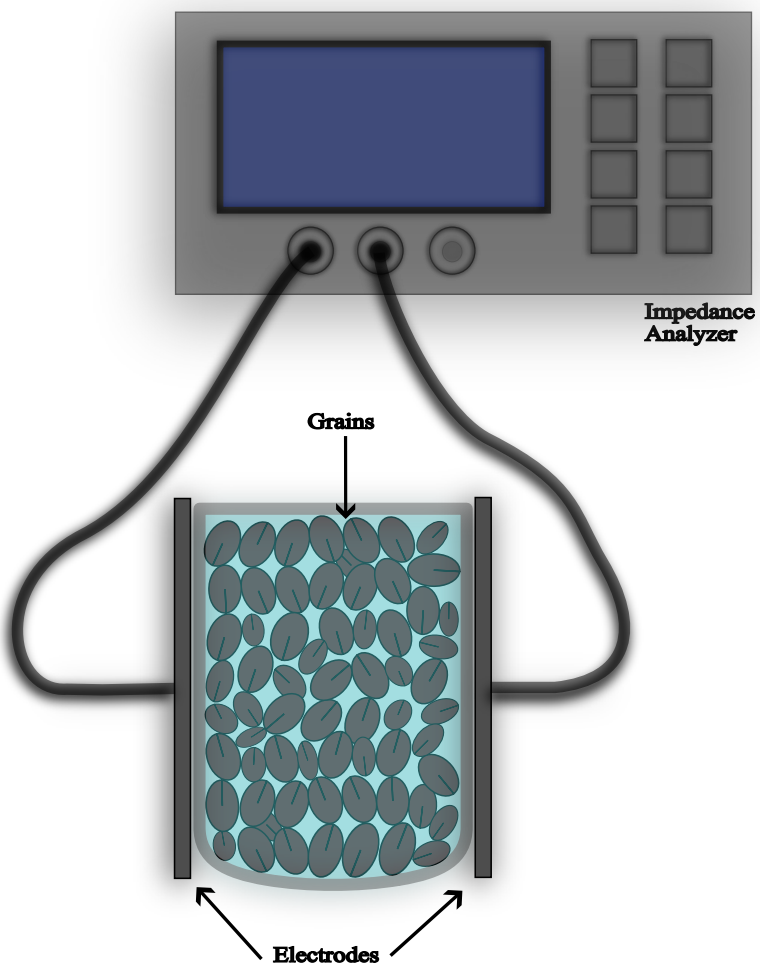

Figure 2.2 – Setup for measurement of moisture content evaluating the resistance of the sample.

The dielectric constant technique [20, 25] allows the grains to be arranged in a structure that acts like a capacitor, as presented in Fig. 2.3. Dielectric variation as a function of the grain moisture is easily observed, since the dielectric constant of water presents stands out over the dielectric constant of air.

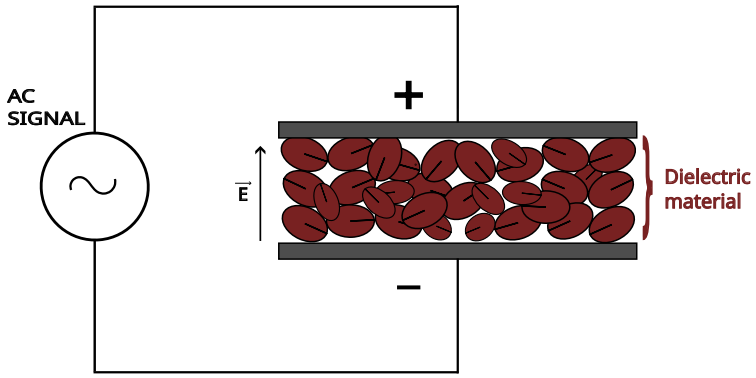

Figure 2.3 – Basis of the moisture measurement as a function of the dielectric value.

Also, microwave technique can be employed to estimate the moisture content of solid samples [26]. It offers advantage over other electromagnetic measurement methods of being non-destructive. The simplified setup is shown in Fig. 2.4.

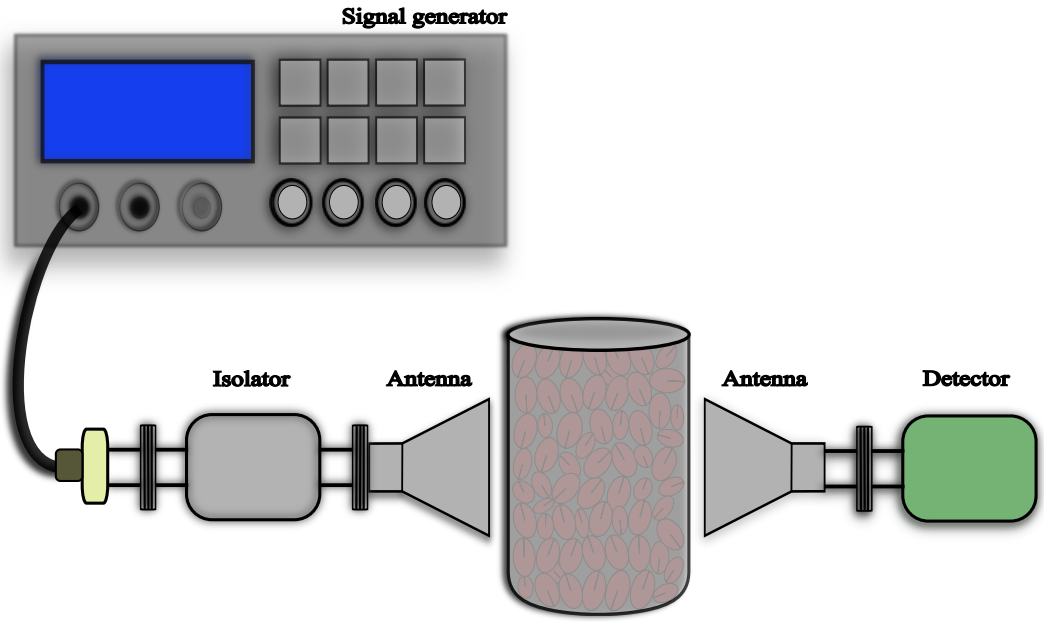

Figure 2.4 – Simpilfied schematic for moisture content estimation by microwave technique.

The magnetic measurement and magnetic resonance imaging techniques, which are concerned with the application of magnetic fields under the grain, are extremely complex techniques that require a specific setup for measurement. The first technique refers to the use of diamagnetic concept of water, in which water molecules generate a repulsive magnetic field in relation to the applied magnetic field. The resultant magnetic field can be related to the moisture content of the material [27]. The second technique is

also complex, once the resonance of the hydrogen atom is evaluated. Through the magnetic moment signal of the hydrogen atom (essentially the spin of the hydrogen proton), it is is possible to trace causality to the amount of water in a sample. The intensity of the captured signal (the spin measurement of the proton) is directly proportional to the amount of water existing in the sample [28]. Finally, this method is considered quite resolute and highly accurate although the setup of this measurement is complex. A simplified schematic of the magnetic measurement is presented in Fig. 2.5.

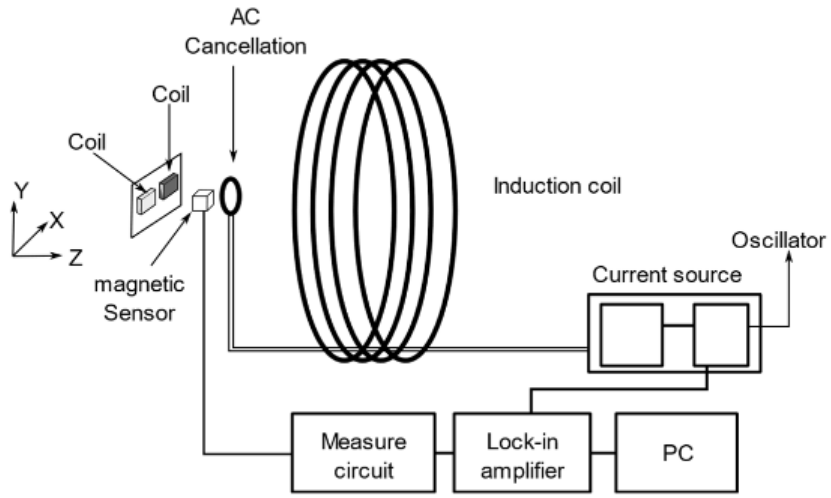

Figure 2.5 – Simplified schematic of magnetic approach for moisture determination [20].

A simplified schematic of the ultra-wide band radar technique is presented in Fig. 2.6. The ultra-wide band radar technique comprises a high energy density signal pulse that uses a bandwidth exceeding 500 MHz or more than 25 % of the center frequency. This signal is emitted into a cylindrical vessel and the reflection coefficient and the complex portion of the grain permittivity are used to evaluate the amount of water in the sample [29]. Analyzing the sample by this method has the advantage of eliminating the influence of the average sample density (bulk density). Bulk density, or apparent density, refers to the average mass of a solid by its volume. The most specific example is with regard to granular materials, since these materials have voids when agglomerated. These voids are usually occupied by a fluid, such as air.

The infrared spectroscopy technique uses the frequency range known as near-infrared (NIR), which is located at the beginning of the infrared spectrum. In this frequency range, organic molecules can absorb the emitted wavelength [20, 29]. As observed in Fig. 2.7, the rate of absorption is directly related to the concentration of these molecules in a sample.

The ultrasonic technique is based on the propagation of acoustic waves through the porous medium in which the grain sample consists [30]. The intensity of the signal that the receiver gets is correlated to the amount of water in the sample, as shown in Fig. 2.8.

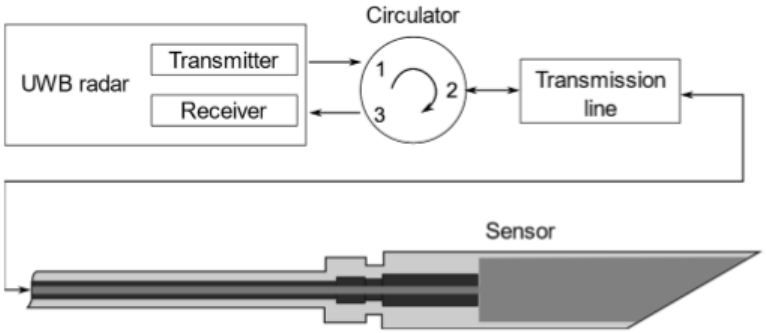

Figure 2.6 – Simplified schematic of ultra-wide band radar approach for moisture determination [20].

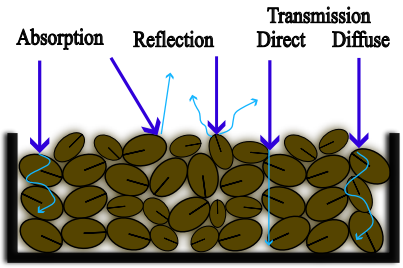

Figure 2.7 – Operation of infrared spectroscopy and hyperspectral imaging principles for moisture content measurement using radiated electromagnetic waves.

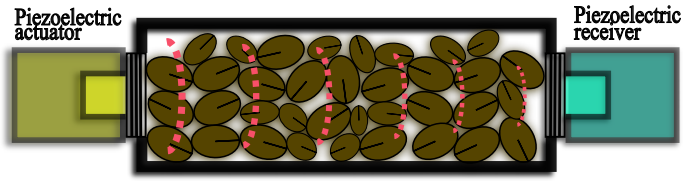

Figure 2.8 – Simplified schematic of ultrasonic technique for moisture determination.

The thermography technique uses radiation emitted in the electromagnetic spectrum of the infrared range [20, 31]. Typically, an infrared temperature camera is employed to collect the temperature of the grain sample and compare it with a standard dry sample. Water can absorb a large amount of energy before increasing its temperature by 1 °C due its high thermal capacity. Consequently, a wet sample will radiate more infrared than a dry sample, inferring the sample's moisture. It is worth noting that this technique generates thermographic images of the sample, under analysis.

The hyperspectral imaging technique consists in using a hyperspectral camera to analyze the reflected frequency spectrum of the material under analysis [32]. This camera allows to obtain the information of the entire spectrum in relation to a single pixel, i.e., for each pixel that forms the collected image, there is information of the entire electromagnetic spectrum. Due to its large capture power, this type of method can be applied for the recognition of irregular materials as well as materials in motion.

Lastly, the relative humidity technique [20, 33] consists of monitoring the water

vapor concentration in an environment. These sensors can be resistive or capacitive and they need to work together with a temperature sensor, once the water vapor content is temperature dependent. These sensors have proven to be efficient when used with 3 to 4 layers of grains. Since the measured variable is the air humidity (water vapor), it is required to relate this variable to the amount of water in the grains.

2.1.4 New techniques

New techniques for determining grain moisture are enhancements of earlier ones that have proven to be very robust, such as dielectric [25, 34]. Further additions of machine learning algorithms and the leverage of neural networks [35] lead to new insights into monitoring, such as moisture prediction and estimation of humidity [36].

The work proposed here directly contributes to the trend of grain environmental monitoring. This method is based on controlling and monitoring the temperature and humidity of the environment where the grains are inserted combined with the external weather environment monitoring.

Aeration is an approach for controlling the atmosphere of the grain using sensors inside and outside the silo, which was used as a reference for this work [6]. Its purpose is to keep a balanced and healthy storage medium in response to weather variations external to the silo, and thus keep the grain storage protected against the presence of harmful microorganisms that may damage the grains. The physical dynamics inside a silo are presented in Fig. 2.9.

2.2 Temperature sensors

2.2.1 Temperature sensing methods

The temperature measurement is performed from one or more sensors, inferring the temperature in their immediate region from the variation of a physical characteristic, such as the dilatation of solids and gases, or from electromagnetic waves. There are four main techniques that use mechanical, thermoelectric, thermoresistive, and irradiation principles [37]. In this work, we will focus on a specific temperature detector inside the thermoresistive group - RTDs, that relates the temperature to the electrical resistance of a metal.

2.2.2 Resistive Temperature Detectors

The technique of RTD measurement essentially deals with the effect of temperature on the electrical resistance of a metal.

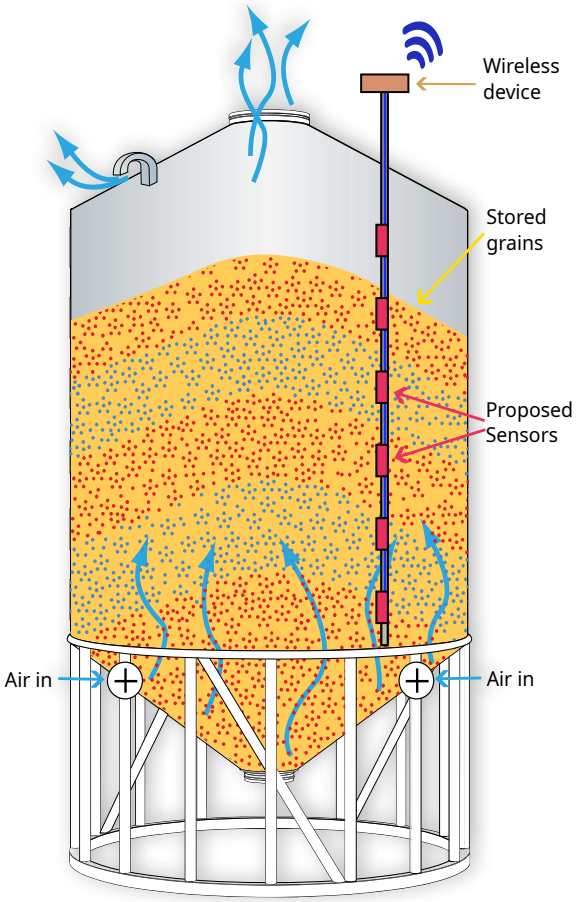

Figure 2.9 – Aerating system for grain environmental controlling.

The molecular movement that happens in metals with a heat source increases their electrical resistance. In this way, by applying a constant electric current to this material, the electrons will have a higher or lower resistance to travel along the conductor as a consequence of the drop or rise in temperature, respectively. As a result, potential difference at the resistance terminals will be inversely proportional to the temperature variation that the metal is exposed to.

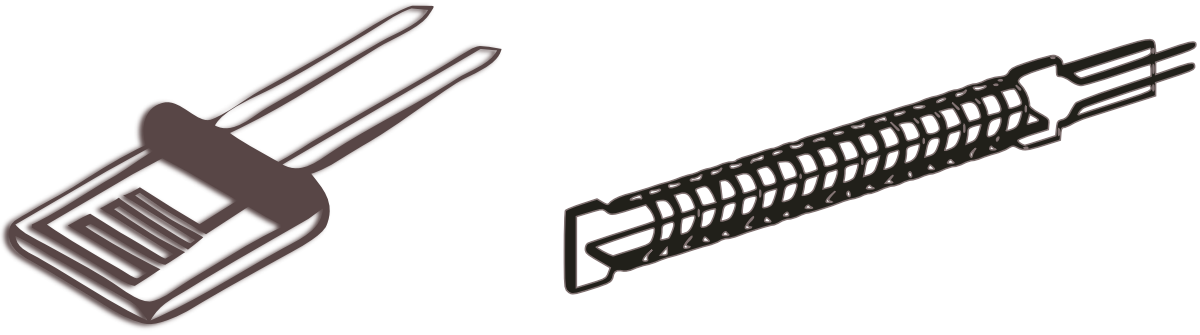

(a) (b)

Figure 2.10 – Resistive temperature detectors. (a) Thin-film elements. (b) Strain-free constructions.

The basic construction of an RTD consists of using a long thin conductive metal covered by a thermal protective layer, such as glass or ceramic. RTD implementations are shown in Fig. 2.10.

The voltage output of a resistance-based sensor is acquired from the wheatstone bridge circuit, in which the sensor is positioned in one of the arms of the bridge. This topic will be explained in details in Chapter 3.

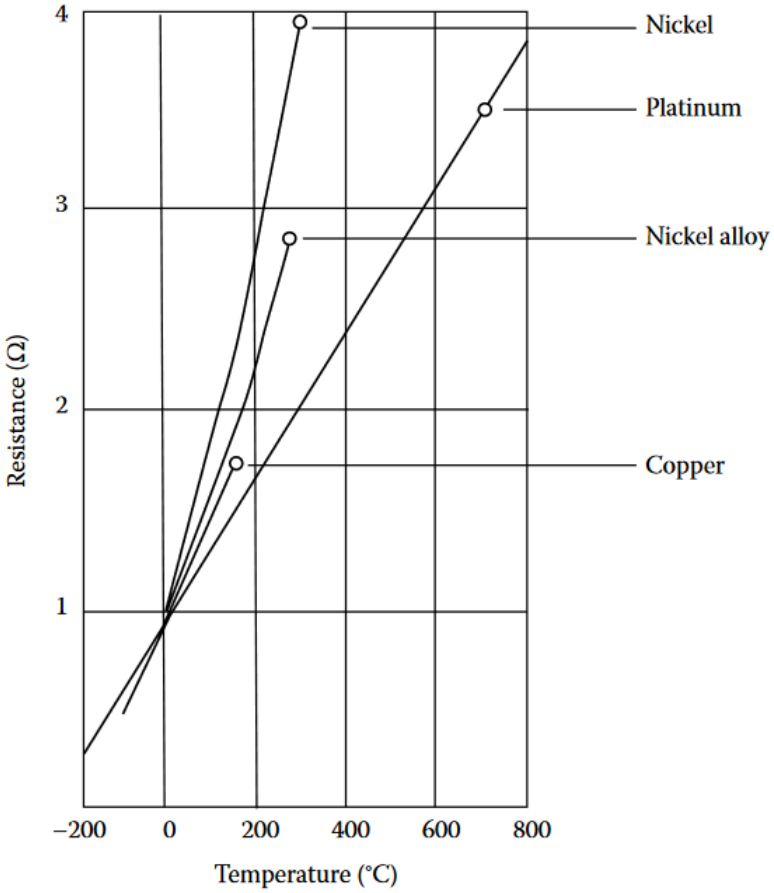

Figure 2.11 – Operating range of different metals used as RTD [38].

The main advantages in the RTD application are linearity and stability over a wide temperature range, as shown in Fig. 2.11. On the other hand, RTDs exhibit very small variations in resistance value as a function of temperature.

In addition, one might assume that since there is a small resistance variation, it is sufficient to use a high value current source in which we can acquire higher voltage values in relation to the low resistance variation - it is not possible. RTD-based sensors are susceptible to self-heating due to the joule effect caused by the flow of electric current. Finally, another disadvantage of this measurement technique involves the use of more than 2 wires to measure the voltage. Since RTDs have small resistance variations, adding wires or pins for connection to the measuring instrument introduces parasitic resistances that must be compensated by a 4-wire measurement.

2.3 Printed circuit board technology

Printed circuit boards are physical structures based on insulating material supporting well-defined metallic interconnections that conduct current between electrical and electronic components. These components are arranged on fiberglass or ceramic substrate. The copper track pattern is defined by the project designer and printed on a substrate [17].

Terminologies such as PCB or PWB are used in the literature to describe the technique of grouping and interconnecting different electrical and electronic components. It is a basic structure, which has been supporting an increasing amount of components and interconnections given the scaling and complexity of the electronic devices we currently use. The role of the substrate in electronic design is so prominent that a specific discipline is dedicated to the studies of enclosures and interconnections to improve the performance of electronic circuits, called electronic packaging [39]. It is a multidisciplinary field in which the study of the integration of electronic systems/components and their interconnection with the substrate is performed. It covers packaging different functions on to a semiconductor chip (Level 0) to connecting host to terminals and other peripherals (Level 5), optimizing the signal integrity while reducing the influence of external events such as temperature, humidity, and mechanical shocks [39].

The Fig. 2.12 presents the major steps in manufacturing a single-sided printed circuit board [40]. Essentially, the print & etch technique is used to fabricate printed circuits. The circuit layout is printed on a base material composed by copper clad laminate and unwanted portions of cooper is etched, then the revealed circuit is protected by a solder mask.

2.3.1 PCB-based sensors

PCB-based sensors are passive electrical components which have their physical characteristics well determined by the designer and can be made application-specific. The conductive tracks are used as electrodes to capture the environmental phenomena. It is also possible to add several materials to the PCB manufacturing process in order to enhance the selectivity for a desireble phenomena.

Sensors based on this technology can be developed in several sizes, high scale and low cost, since they can be made following the steps presented in Fig. 2.12. Besides the cost reduction, these sensors can be easily customized, providing design flexibility and reliability for different applications.

In their simplest form, these sensors consist of applying the PCB fabrication process and using the conductive tracks as electrodes protected from humidity, temperature, and numerous other benefits that materials described in [17] can provide to this substrate as

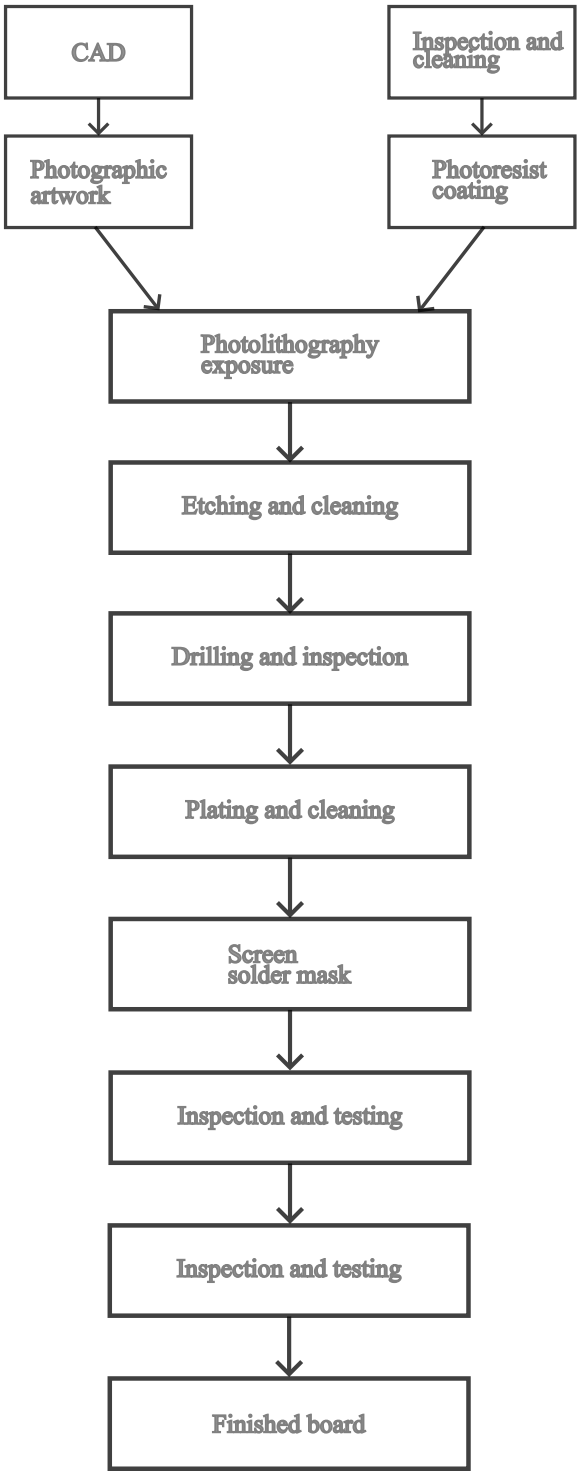

Figure 2.12 – Major steps in manufacturing a single-sided printed circuit board.

a sensing structure. In this way, different sensors can be fabricated, including temperature, pressure, humidity, and gas sensors [41].

Capacitive sensors can be found in application, such as intravenous monitoring [42], nondestructive in situ detection of the kernel moisture content (MC) in corn ears in the field [43] water pollution [44], and dairy products [45].

Capacitive sensors are also used in environmentally friendly processes. The

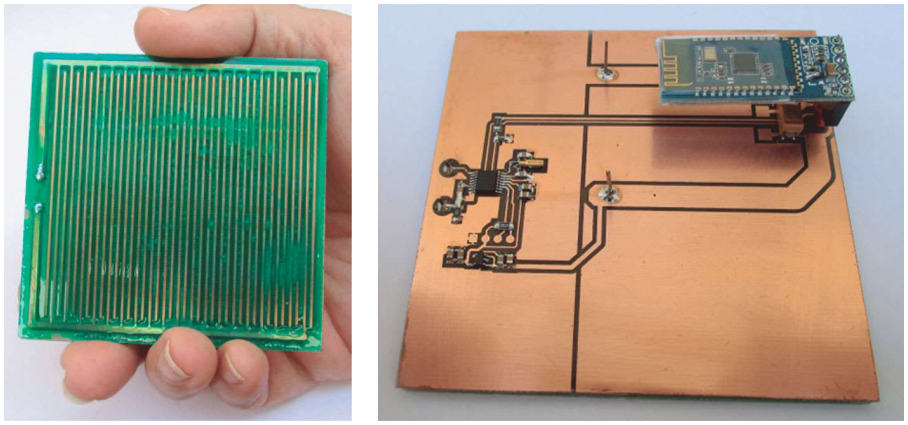

Figure 2.13 – PCB smart sensor: (a) bottom side and (b) top side [25].

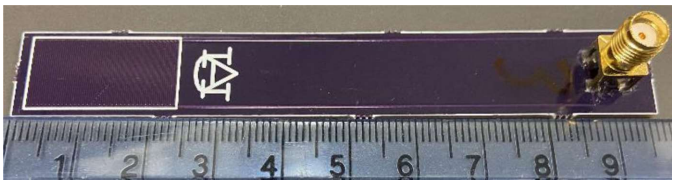

Figure 2.14 – Proposed sensor to detect ice formation events [46].

work presented by Morais, Flávio, et al [25] describes a capacitive smart sensor based on PCB that is able to measure water content in a paper pulp at paper machines processes. The proposed sensor, presented in Fig. 2.13, is based on the operation of fringing field capacitance, which is composed of coplanar electrodes that interact to their surround. The electrode structure is realized in the top Cu layer and covered by a solder mask. The sensor was evaluated in the 20 °C to 40 °C temperature range and can detect water content in the range of 90 % to 92 %. The evaluated range of temperature and water content seems to be suitable for the paper making machine, enabling the reduction of waste earlier in the manufacturing process.

Environmental events like ice melting and inorganic materials deposition can be monitored using capacitive sensors. Dean, Robert N. [46] proposed a capacitive interdigitated electrode structure realized in PCB for detecting ice events. The prototype is presented in Fig. 2.14. The PCB sensor structure has the same material properties described in the previous work, which enables the Cu electrodes on top layer to interact with their surround by means of fringing field capacitance and it is protected by polymeric solder mask. Therefore, the author evaluated the ratio of measurments done using deionized water at 1 kHz and 64 kHz. The measurement results for dry (23 °C), wet (34 °C to 5 °C) and icy condition(0 °C to −30 °C) were sucessfully described.

As a contaminant in water, inorganic materials can also be detected by means of interdigitated capacitive sensor [47]. When in contact with water bulk, an accumulation of ions species in its interface creates an electric double layer due to the potential

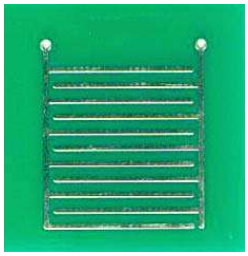

Figure 2.15 – Wang, Xiaolei, et al proposed sensor [47]

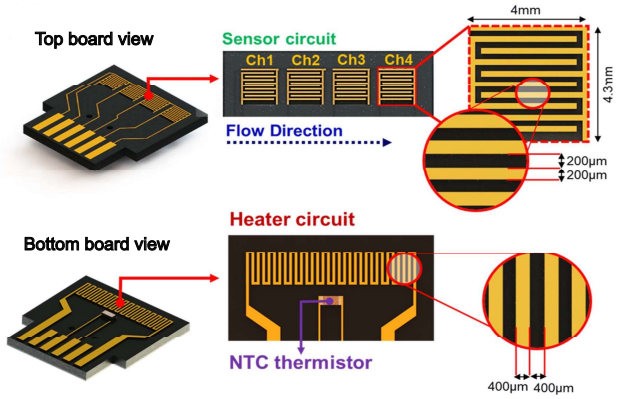

Figure 2.16 – Interdigitated electrode developed by [48].

difference between them. Also a resistance path is created in water bulk. The sensor was evaluated at frequency of 5 kHz at 25 °C and the algorithm guaranteed that the optimal sensing electrodes always dominated the measurement, resulting in a conductivity range of 0.5 μS/cm to 500 mS/cm. The sensor is shown in Fig. 2.15.

Whether indoors or outdoors, highly selective gas detection plays a key role in detecting toxic volatile organic compounds (VOC) that are emitted into the atmosphere from the use of fossil fuels in transportation and industrial processes, as well as preventing human exposure to certain flammable and harzadous gases into different sectors. The reconfigurable PCB graphite-based interdigitated gas sensor proposed by da Costa, João Paulo de Campos, et al. [48] was able to detect acetone, methanol, isopropanol, ethanol, and chloroform gases with stability and repeatability. It was used double-sided, 2-oz-thick copper-clad FR-4 substrate with a gold coating (according to IPC-4552) to improve the performance. The proposed sensor is shown in Fig. 2.16. It was evaluated the effects of graphite as a sensing material, which promises an increase in sensitivity and selectivity at low cost for room-temperature applications. The graphite solution was sprayed at appropriate parameters described in the paper. Based on the conductivity parameter of the gas sensors, the chronoamperometry technique was applied in order to follow the changes in the electric current due to the adsorption process that occurs on the graphite surface. The sensors presents a sensitivity of approximately $\pm 100\,\mu$A, $\pm\ 60\,\mu$A, $\pm$ 40 μA,, $\pm 20\,\mu$A, $\pm 10\,\mu$A at a 200 ppm for acetone, methanol, isopropanol, ethanol, and

chloroform gases respectively.

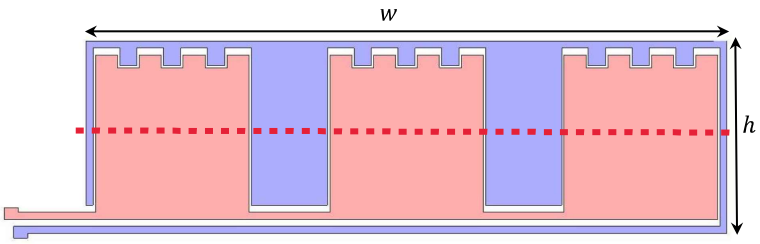

Figure 2.17 – Sensor strucuture proposed by [49].

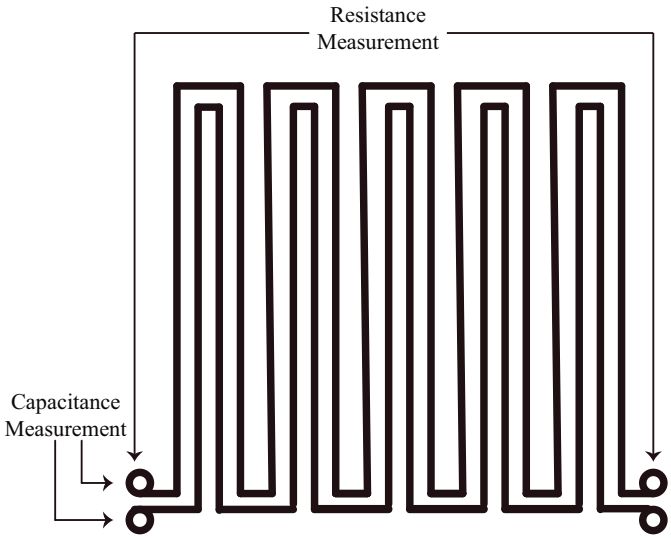

Figure 2.18 – Reconfigurable sensor for measuring temperature and moisture proposed by [34].

Another important environmental monitoring application is related to agriculture production and food storage. In this subject, PCB capacitive sensors can also be employed to monitor granular materials, such as soil, sand and grains. These sensors explore the fringing field created by coplanar electrodes and it can be used to measure dielectric constant of different granular materials by means of fringing field capacitance measurement. However, these sensors suffer from a source of uncertainty related to the random distribution of the grains and air between them. In order to improve the accuracy of measurements, Corradi, Riccardo Ferretti, et al. [49] proposed a new coplanar sensor geometry optimized by numerical simulations in order to track contaminants in seeds. Experiments were performed at 5kHz using rice and sunflower seeds, and reductions in standard deviation of 20 % compared to a conventional interdigital electrode structure were presented. The proposed sensor is shown in Fig. 2.17.

The efficient storage of grain is essential for sustainable agriculture. It plays a vital role in the preservation of natural resources, the conservation of their quality, and the preservation of the commercial value of the grain. Successful storage for long periods demands controlling of its moisture content and temperature, slowing mold growth and

inhibiting insect activity. The reconfigurable PCB multisensor proposed by dos Santos, Adelson, et al. [34] was designed on conventional FR-4 substrate. Instead of using a traditional interdigitated structure, it was implemented two parallel Cu electrodes that cover the complete area of the PCB alongside each other, as shown in Fig. 2.18. By reconfiguring the sensor electrodes, it is possible to evaluate the capacitance of two parallel Cu track or the resistance of a single electrode. These sensor elements are used to measure both moisture content and temperature, respectively. The sensor was evaluated over a moisture content range of 5.2 % to 22.2 % at 21 °C and the temperature range of 10 °C to 50 °C, with an average capacitance range of 14.6 pF and sensitivity of 0.98 pF/% for the former and nonlinearity error of 0.64 °C for the latter.

The conservation of grain quality is also the subject of study for long-duration manned space missions. In that way, Dean, Robert N., et al. [19] explores the high permittivity of water compared with the relative permittivity of organic materials in order to capacitively measure moisture content of stored grains. The working principle is similar to the work described above, although an interdigitated capacitive sensor has been implemented on PCB. The PCB sensor was evaluated by several measurements of its capacitance at 250 kHz in a bowl filled with corn kernels at 21 °C in the range 9 % to 27 %, resulting in an increase of 2.5 pF over the evaluated range with linear behavior. The Fig. 2.19 shows the fabricated sensor.

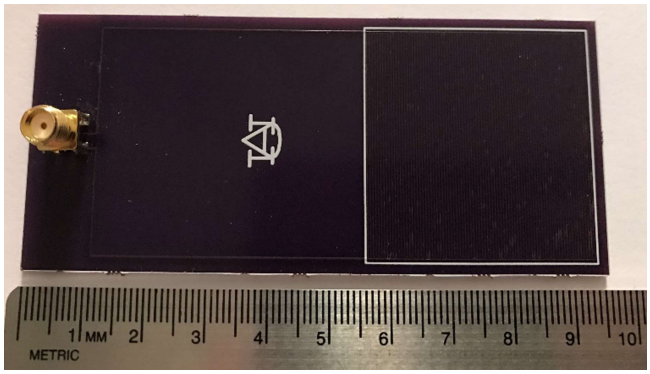

Figure 2.19 – Interdigitated capacitive sensor proposed by [19].

As well as in touch with different grains, humans have been in constant exposure to other different kinds of organisms, such as viruses, fungi, and bacteria. Interdigitated sensors can also be applied in biomedical field. The work of Vasiljevic, Dragana Z., et al. [50] presented in Fig. 2.20 describe the design and characterization of non-invasive PCB sensor for detection of different concentrations of bacteria such as Pseudomonas aeruginosa and Staphylococcus aureus. Through resonance frequency, it is possible to differentiate these bacteria in a physiological saline to provide rapid identification from biological samples. In addition to that, intravenous fluids and the measurement of their drip rates can be taken advantage of PCB sensors.

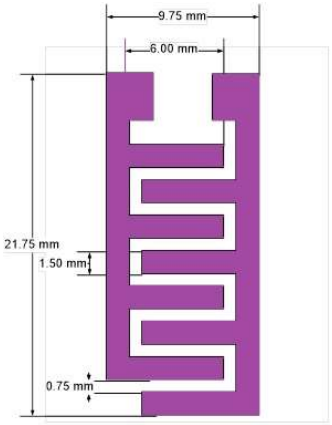

Figure 2.20 – PCB sensor proposed by [50] for bacteria detection.

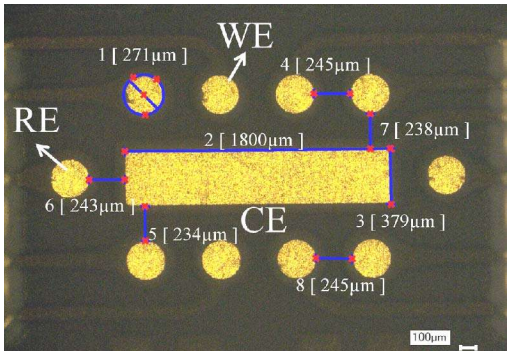

Figure 2.21 – PCB based sensor for glucose measurement [51].

Apart from microorganism detection, PCB technology can support the development of biosensors, such as glucose sensors. Glucose sensors have remarkable popularity and have transformed diabetes management and the monitoring of a wide variety of medical conditions. Thus there are efforts to develop a low-cost, mass-manufacturable solution for such a sensor. A multi-electrode array based on PCB technology was developed by Kassanos, Panagiotis, Salzitsa Anastasova, and Guang-Zhong Yang [51] in order to detect relevant biomolecules or chemical compounds that improve glucose measurement. The amperometric technique is an electrochemical sensing method used to detect and quantify analyte concentration in a sample. The electron transfer occurs in a sample solution that has a selective electrode (WE), a reference electrode (RE) and an auxiliary electrode (SE). The reference electrode provides stable potential for the selective electrode, so the selective electrode interacts with the sample solution, leading to a change in the electrical current flowing through the selective electrode and auxiliary electrode. Therefore, by measuring the electric current generated by an electrochemical cell it is possible to quantify the analyte concentration. The Fig. 2.21 presents the proposed PCB sensor.

Despite temperature and humidity monitoring, coastal regions have different environmental scenarios, due to the proximity of salty air or saltwater. Salty environments can produce rust from iron and steel structures, damaging building structures and dumping

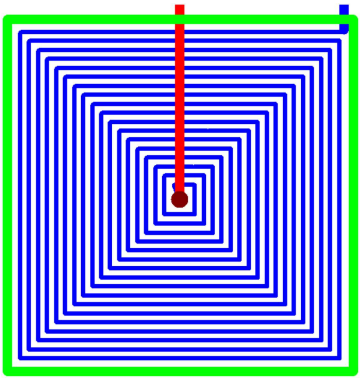

Figure 2.22 – Drawing of the sensor (blue: topside metal, red: backside metal, green: silkscreen, tan: plated via) [52].

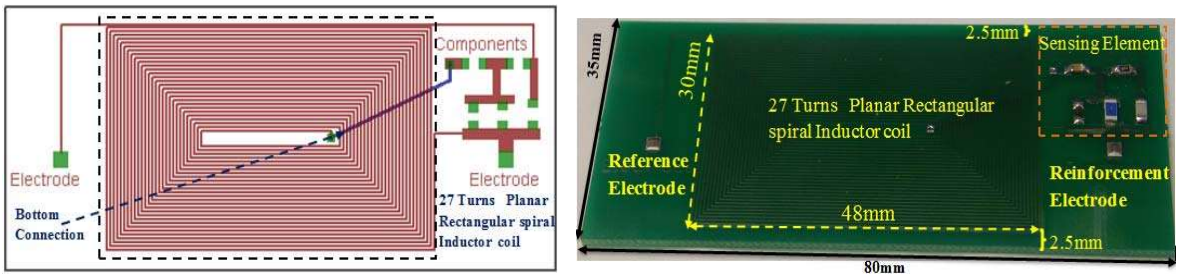

(a) (b)

Figure 2.23 – (a) Drawing of the sensor. (b) Sensing circuit. [53].

their sediments in the sand. Early warning sensors can be employed for monitoring the corrosion rate and predictive maintenance can be implemented in order to reduce infrastructure management and public safety issues. The work presented by Dean, Robert N., Michael J. Bozack, and Rachael C. Tighe [52] describes the design and fabrication of an inductive planar sensor for this purpose. The sensor is presented in Fig. 2.22, and it was fabricated using traditional PCB FR-4 substrate, in which Cu traces operate as inductor windings and the solder mask for protecting the sensor. The basic operation of this sensor exploits the proportionality between relative magnetic permeability of materials and inductance. When the windings are close enough to high relative permeability materials, such as iron and steel, their inductance increases. The proposed sensor was evaluated over a frequency range of 500 kHz to 7 MHz using different materials, such as air, natural rust, pure ferric oxide among others.The authors also evaluated using dried beach sand.

A similar sensor is shown in Fig. 2.23. It was proposed by Perveen, Khalada, et al. [53], in which an inductive planar sensor based on PCB was designed to monitor corrosion potential wirelessly. It was implemented as an inductively coupled coil, in which there was an interrogator coil and the PCB sensor coil. The sensing technique is based on a passive LC coil resonator, in which the resonant frequency varies due to the change of the varactor junction capacitance. Two electrodes were used as a galvanic cell embedded in concrete and the potential produced by corrosion control the varactor capacitance, therefore changing the resonant frequency. The corrosion tests reported sensitivity of

≈ 1.2 kHz/mV and resolution less than 10 mV, and resonant frequency of zero corrosion of 5.930 MHz.

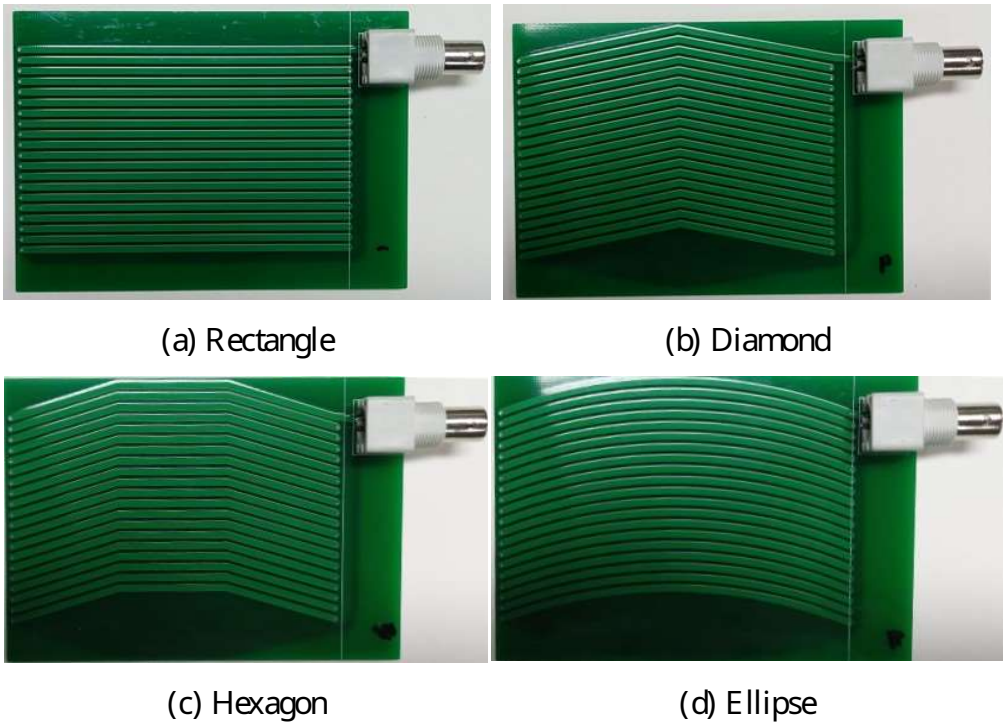

Figure 2.24 – Four PCB structures evaluated by [54].

The PCB sensors were studied for corona partial discharge measurements. Operating at high voltages, transformers, cables, joints among other high voltage components are sensitive to insulation deterioration and early detection of this breakdown can prevent power distribution failures as well as human injuries. Corona partial discharge (PD) occurs when molecules around the surface of a high voltage conductor ionize and become conductive due to the strength of the electric field. Partial discharge can occur between the insulation and the conductor, causing long lasting damage over time and potential insulator rupture. Different types of Rogowski coil sensors (RCSs) based on PCB were evaluated in Kim, Sung-Wook, et al. [54] and their performance for PD measurement were discussed. The structures is presented in Fig. 2.24. Strucures such as rectangle, diamond, hexagon, and ellipse were designed using PCB technology in order to get low manufacturing cost and high reliability. PD signals are characterized by high frequency components (up to few GHz) and low amplitude. Exploiting the electromagnetic induction of RCS, the authors acquired the induced voltage in the coil due to the high frequency electromagnetic field generated by PD. Through experiments to determine linearity and sensitivity, the authors concluded that the hexagon structure provided the most promising results, being a strong replacement for expensive commercial PD sensors.

Moreover, the experimental investigation conducted by Imburgia, Antonino, et al. [55] regarding PD applied different sensor shapes compared to the previously described work. This work comprises the analysis of two PCB inductive sensors with non-spiral and

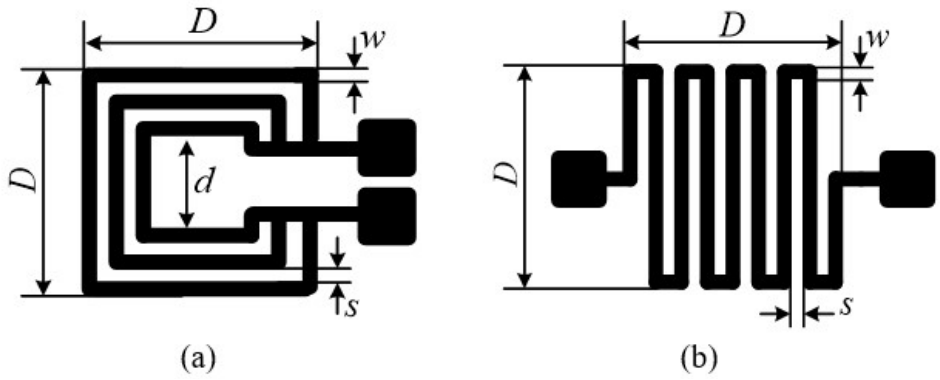

Figure 2.25 – Evaluated inductive sensor topologies: (a) non-spiral and (b) meander. [55].

meander design. Through software simulation and experiments, the authors conclude that both sensors have the highest sensitivity when they are placed at 90 °C to the PD source. The experimental test exposed both sensors to electromagnetic waves generated when applying the lowest voltage at which partial discharges are observed (3 kV), resulting in a frequency spectrum of 35 MHz for both sensors, approximately. The two PCB inductive sensors were presented in Fig. 2.25.

The performance of Cu trace current sensing method for power electronics is conducted by Ziegler, Silvio, et al. [56]. It investigated the static and dynamic performance of a PCB trace operating as a shunt resistor. The authors used a busbar as a Cu trace in order to monitor current levels of hundred amperes. As expected, high currents generate heat. Temperature drift has been overcome through temperature monitoring of the busbar by a microcontroller interface and two correction algorithms were evaluated. The bandwidth of the proposed sensor was dominated by mutual inductance. Therefore, a RC low-pass filter was introduced in order to extend the bandwidth by several decades above 2 kHz. Results showed that in order to achieve 1 % of accuracy in current measurement over a temperature range of ± 75 K the temperature sensor needs to be better than ± 3.3 K to properly compensate for the joule effect.

3 Multisensor for Moisture and Temperature Measurement based on PCB Technology

In this chapter we present the design and the performance of a reconfigurable multisensor comprising a copper RTD and a fringing field capacitor based on PCB Technology.

3.1 Capacitive sensor

Capacitance is an electrical foundational property which arises where two parallel conductors are separated by a dielectric. Once a voltage is applied across the conductors, the electric field within the dielectric is generated and the bound electric charges are polarized, or moved from their equilibrium position due to displacement currents. The dielectrics that rely on highly polar molecules will have a higher dielectric constant. Under a DC voltage, displacement currents only flow shortly enough to spread charges and store them in the immediate area surrounding the conductors between the dielectric. Conversely, an alternating displacement current keeps moving in the presence of an AC voltage, whereby its magnitude depends on the frequency of the signal. The reordering of the electric charges will lead to a stored charge between the conductors, whose amount of charge will depend on the voltage, the time, and the total energy available.

Considering these two conductors as planes, each of area A, separated by distance d, the generated electric field and charge distribution will be even throughout all points that are not adjacent to the borders, as presented in Fig. 3.1. Therefore, we can write the capacitance as demonstrated in Eq.(3.1), where ϵ is the complex frequency-dependent permittivity of the material.

$$C = \epsilon \frac{A}{d} \tag{3.1}$$

At the edge of the parallel plate, the electric field is distorted and its equipotential line uniformity disappears. This is known as the fringe field effect and takes place in any closely spaced conductor.

One can use such behavior to design capacitive structures in which fringe effect dominates the capacitance value. On top of that, capacitive transduction in microelectromechanical systems (MEMS) applications as well can exploit the fringe field effect given the capability of building small-sized capacitors with high capacitance values, thus

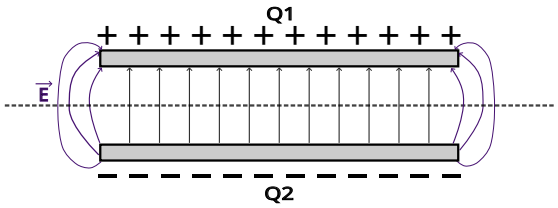

Figure 3.1 – Charge distribution and resultant electric field generated by two parallel conductors.

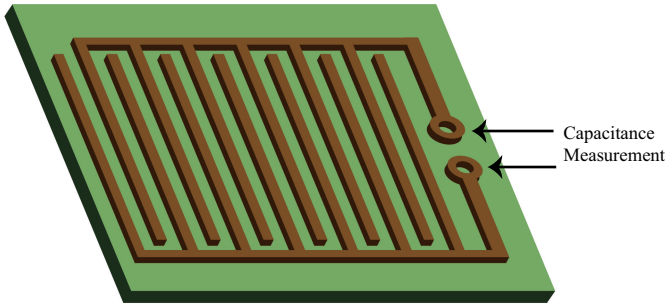

Figure 3.2 – Conventional PCB fringing field capacitance sensor.

providing an important feature in such systems as the dimension decreases from micro to nanoscale [57].

A typical fringing field capacitive sensor is built of interdigitated coplanar electrodes made of copper traces from a printed circuit board, as shown in Fig. 3.2. It comprises two interconnected sets of metallic fingers, each set connected to an electrode, forming a capacitor array. The fingers are placed in a tooth comb-like pattern and they are separated by a dielectric material. The distance separating the fingers is usually very small, which allows a large capacitance to be obtained in a small area.

The capacitance of a structure with fingers of length l, distance between two fingers d, thickness of the copper h, and n fingers, is given by Eq.(3.2), where ϵ_0 and ϵ_r are, respectively, the permittivity of free space and the relative permittivity of the dielectric material between two fingers.

$$C = \epsilon_r \epsilon_0 \frac{nlh}{d}, \tag{3.2}$$

The value of the capacitance changes if a material with a different ϵ_r is placed in contact with the PCB surface. This type of sensor has already been used to measure moisture and it has been shown that the capacitance of the PCB fringing field capacitors have a dependence over temperature, presenting a sensitivity of $\approx$ 0.114 %/°C [58]. Therefore, it is imperative to use another sensor (a temperature sensor) to measure the temperature and correct for the capacitance measurement.

3.2 Temperature sensor

The operation of the RTD is predicated on the measurement of the electrical resistance of a metal wire (or thin film), usually platinum, nickel or copper, as these materials have a positive resistance temperature coefficient (TC) and their electrical resistance is predictably changing in an essentially linear and repeatable fashion, as shown in Fig. 2.11 in Chapter 2.

If a constant small current flows through the metal, the resulting voltage drop in the material is dependent on the value of the electrical resistance according to Ohm's law. Once the resistance R_0 of the metal wire is known at a given temperature, any change in temperature will provide a proportional change in the value of the resistance. Therefore, a small voltage drop due to $R_0 \pm \Delta R$ can be conditioned to provide the temperature measurement readout. Considering a material with a resistance R_i at a temperature T_i has a linear thermal resistance coefficient given by:

$$\alpha = \frac{1}{R_i}\frac{dR}{dT} \tag{3.3}$$

The resistance of the material as a function of the temperature can be written as:

$$R\left(T\right) = R_i\left[1 + \alpha\left(T - T_i\right)\right], \tag{3.4}$$

for $T = 0\,^{\circ}\mathrm{C}$, the value of $R(T)$ is R_0, the equation is simplified to:

$$R\left(T\right) = R_0\left[1 + \alpha T\right] \tag{3.5}$$

Although copper presents low TC, it has been presented copper resistance temperature detector with excellent linearity [59, 60, 61]. Thus, a confident compensation for capacitive measurements can be realized with a copper RTD.

Therefore, for a Cu PCB track with length l, thickness h, width w and electric resistivity ρ the resistance can be written as:

$$R = \rho\frac{l}{w.h} \tag{3.6}$$

3.3 Multisensor design

This section is partially reproduced from the paper "Proposal of a Reconfigurable Sensor for Measuring Temperature and Capacitance.", published in the 6th International Conference on Sensors Engineering and Electronics Instrumentation Advances (SEIA 2020), 18. ©2020 IFSA Publishing.

Leveraging the complete PCB supply chain, PCB-based sensors can be easily designed and manufactured at low cost using open-source EDA. The project was made using the KICAD, both for multisensor strucutre and its electronics. The new pattern is made using two parallel long copper tracks, with a serpentine shape, as presented in Fig. 3.3.

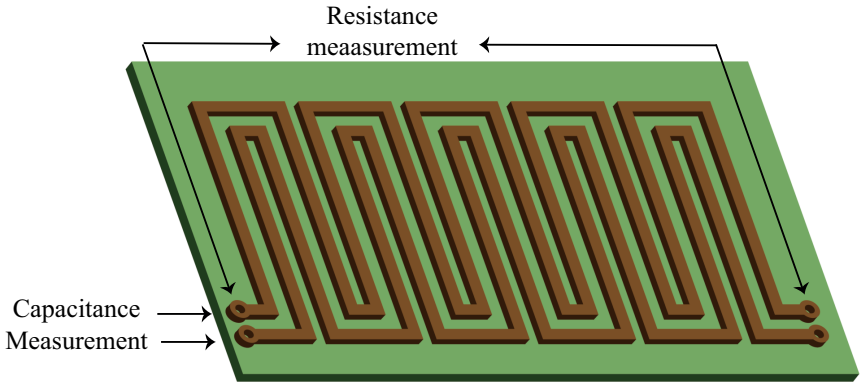

Figure 3.3 – Modified structure of a capacitive and RTD reconfigurable sensor.

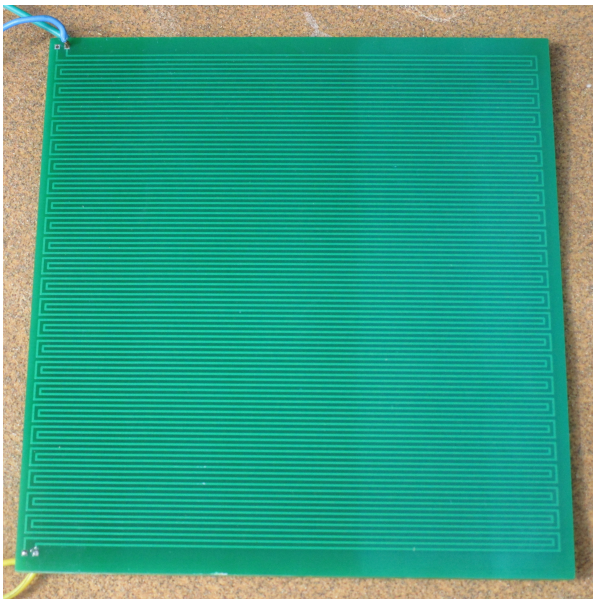

Figure 3.4 – First Multisensor prototype.

The sensor was initially fabricated using 2-layer FR-4 PCB sided 96 mm x 92 mm, with thickness of 1.6 mm and copper thickness h of 35.6 μm. The PCB sensor has

100 copper tracks (fingers) that run over its extension by a length l of 90 mm, width w of 0.5 mm and are separated by a distance d of 0.5 mm, as shown in Fig. 3.4.

The value of w and l was chosen by defining a resistance value in order of tens of mΩ. The $\frac{w}{d}$ relationship was chosen based on the conclusions presented in [62], that found that using $w = d$ maximizes the value of capacitance per unit area. We used $l \gg d$, resulting $lh \gg d^2$, and therefore the fingers can be considered infinite [62, 63].

Using this new configuration, depending on which points we make contact with the PCB tracks, it is possible to make the conventional capacitance measurement, or measure the resistance of one of the continuous copper tracks. Making contacts at the beginning (or end) of the two parallel tracks, we make the conventional measurement of capacitance. Otherwise, If we make contacts at the beginning and at the end of any of the single continuous tracks, we have a RTD composed of a long line of copper, and we can measure its resistance.

3.4 Resistive Temperature Detector Measurements

This section is partially reproduced from the paper "Proposal of a Reconfigurable Sensor for Measuring Temperature and Capacitance.", published in the 6th International Conference on Sensors Engineering and Electronics Instrumentation Advances (SEIA 2020), 18. ©2020 IFSA Publishing.

The multisensor was inserted in a thermal chamber and a LM135A temperature sensor was placed in contact with it. The resistance R_T of the PCB copper tracks was measured in the $T = 9\,°C$ to $T = 50\,°C$ range, with a Keithley 177 digital multimeter. The 4-wire sensing method was applied to eliminate the influence of cabling.

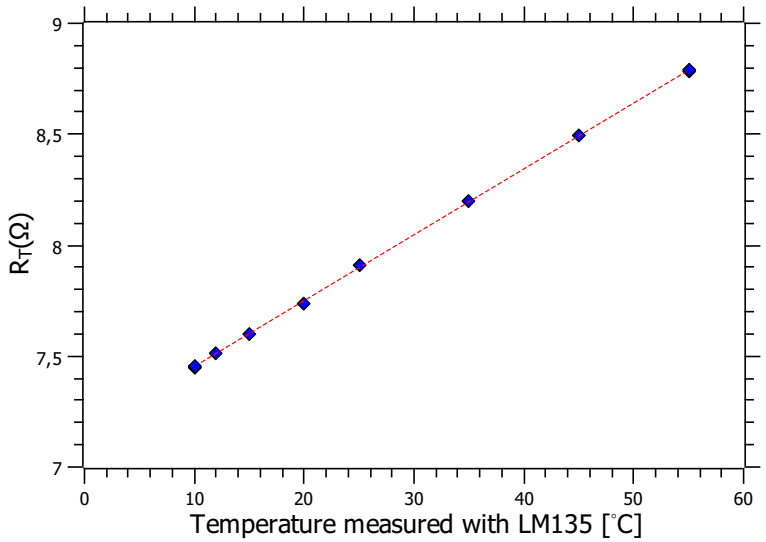

Figure 3.5 – Cooper tracks resistance in function of temperature.

From the plot of Fig. 3.5, the copper resistance in function of temperature can be written as:

$$R(T) = 29.727 \times 10^{-3}.T + 7.154 \tag{3.7}$$

On the first design, it was measured the continuous track of copper $R_0 = 7.913\,\Omega$ at $T_0 = 25\,°\text{C}$. Rearranging the Eq. (3.3), in which $\alpha \approx 0.00420\Omega/°\text{C}$:

$$\frac{dR\,(T)}{dT} = 0.00332\Omega/°C \tag{3.8}$$

3.5 Capacitance measurements

This section is partially reproduced from the paper "Proposal of a Reconfigurable Sensor for Measuring Temperature and Capacitance.", published in 6th International Conference on Sensors Engineering and Electronics Instrumentation Advances (SEIA 2020), 18. ©2020 IFSA Publishing.

The fringing field capacitance was measured in a transparent container with a rule fixed to its edge and then filled with tap water in several steps. At each step, the water level gradually increases, covering a larger area of the sensor surface. The capacitance terminals of the sensor were connected to a GenRad 1659 RLC Digibridge. A photograph of the sensor inserted inside the container partially filled with water and the measured results are presented, respectively in Fig. 3.6 and Fig. 3.7.

From the measurements presented in Fig. 3.7 a capacitance between 300 pF and 500 pF, equivalent to approximately 10 % to 50 % of the sensor area, it is feasible to launch the design of a signal processing circuit for moisture content measurements.

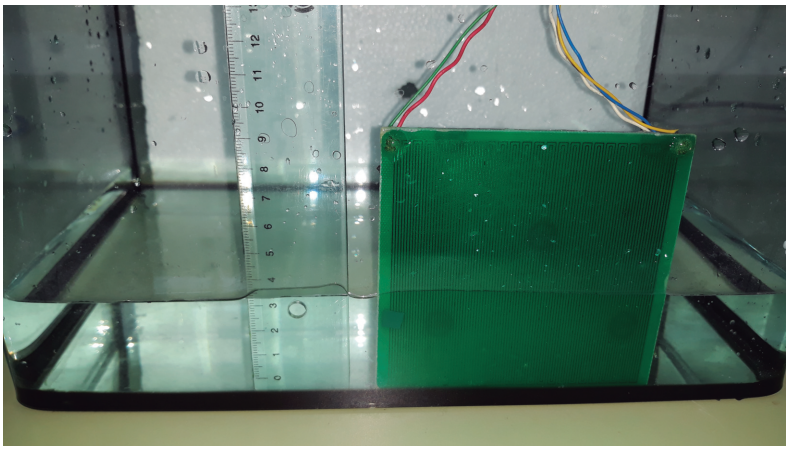

Figure 3.6 – Measurement set-up used for the capacitance test.

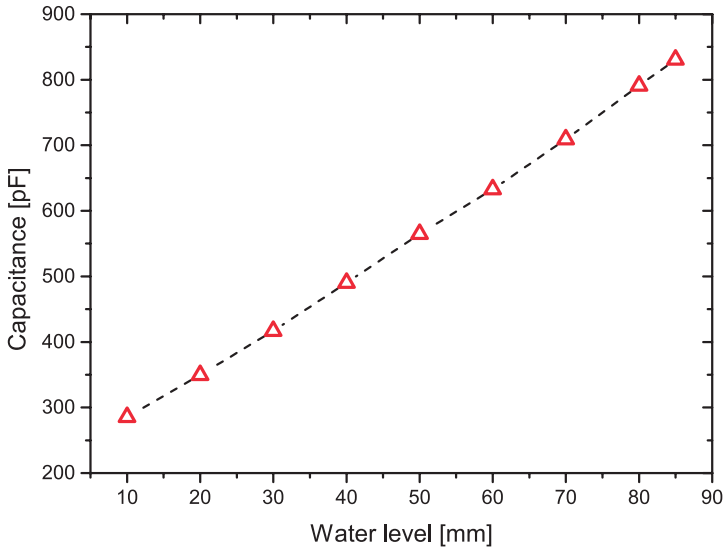

Figure 3.7 – Measured capacitance as a function of the water level.

3.6 Partial conclusions

A prototype of the proposed reconfigurable PCB sensor based on a modified fringing field capacitor and a copper RTD was designed, fabricated and tested in laboratory. This sensor may be used in applications such as soil moisture, air humidity and paper pulp water content, that demands capacitive measurements. Also, the reconfigurable sensor can measure temperature with high precision by means of the copper tracks of PCB operating as an RTD.

The PCB sensor strucuture proposed seems a feasible option to design reconfigurable architectures, since the signal processing circuits can be designed and implemented on the bottom layer of the PCB. Futhermore, the measured results for capacitance and temperature of the fabricated strucutre were in reasonable accordance with the theoretical models.

4 A Reconfigurable Multisensor for Monitoring Stored Grains

In this chapter we present the design of a RTD and a fringing field capacitor based on PCB. Both sensors were fabricated on the same FR-4 substrate of a double-sided PCB. Interconnected to the sensor elements on the opposing side of the PCB, the electronics circuitry for each sensor conditioning, power supply, switching between the sensors and their interface with the microcontroller will be discussed.

4.1 Temperature and Moisture Content Measurement in Precision Agriculture

As discussed in Chapter 2, there are many instruments that are able to provide moisture content (MC) measurements with different techniques. Most of them were designed with small sensing area, leading to measurement of very small samples of grains.

A successful aeration technique is achieved when you can measure the MC at the largest feasible points within the silo. The partial results from Chapter 3 enabled the investigation of this measuring application, as a low-cost and large sensing area solution can allow the averaging of the MC of a large number of kernels when many sensors are distributed inside the silo.

4.2 Reconfigurable Multisensor for Moisture and Temperature Measurements

This section is partially reproduced from the paper "Reconfigurable Sensor Based on PCB Technology for Moisture and Temperature Measurement.", published in Sensors & Transducer (2020), (246) 7, 1-8. ©2020 IFSA Publishing

4.2.1 Signal processing circuits

The temperature data of the PCB copper tracks was acquired using a simple amplifier circuit. The schematic for temperature acquisition is shown in Fig. 4.1.

A constant current source is implemented by means of an OPA192 operational amplifier (A2), a LM285-1.2 voltage reference, a resistor R_2 and a PNP transistor (Q1).

The voltage on R_T is sent to an INA125 instrumentation amplifier, in which offset and the gain are adjusted by a potentiometer and by a inverter amplifier, respectively.

The moisture content data was acquired using a single relaxation oscillator circuit. The schematic for moisture acquisition is shown in Fig. 4.2.

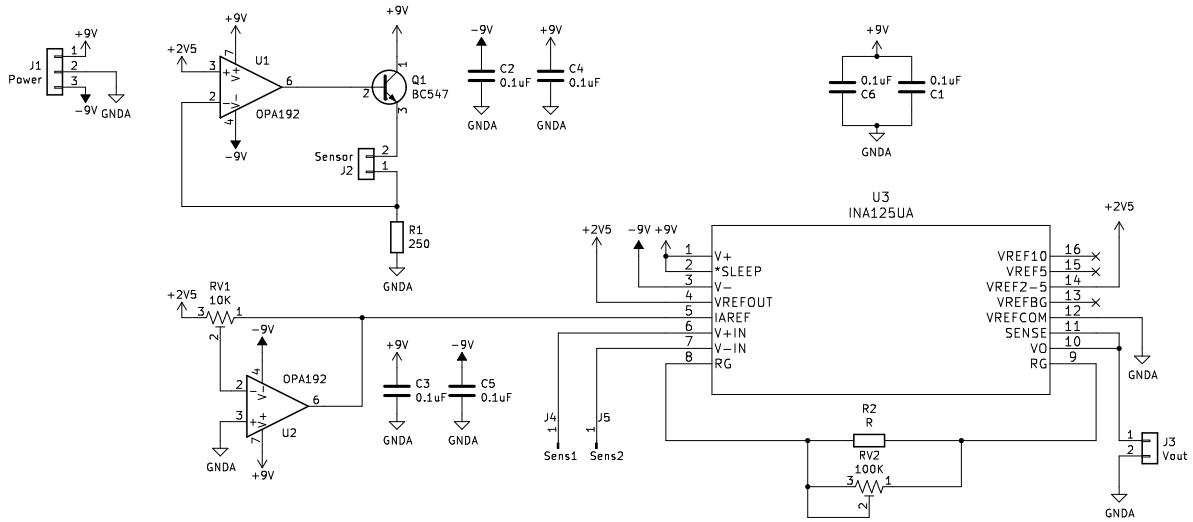

Figure 4.1 – Schematic for temperature acquisition.

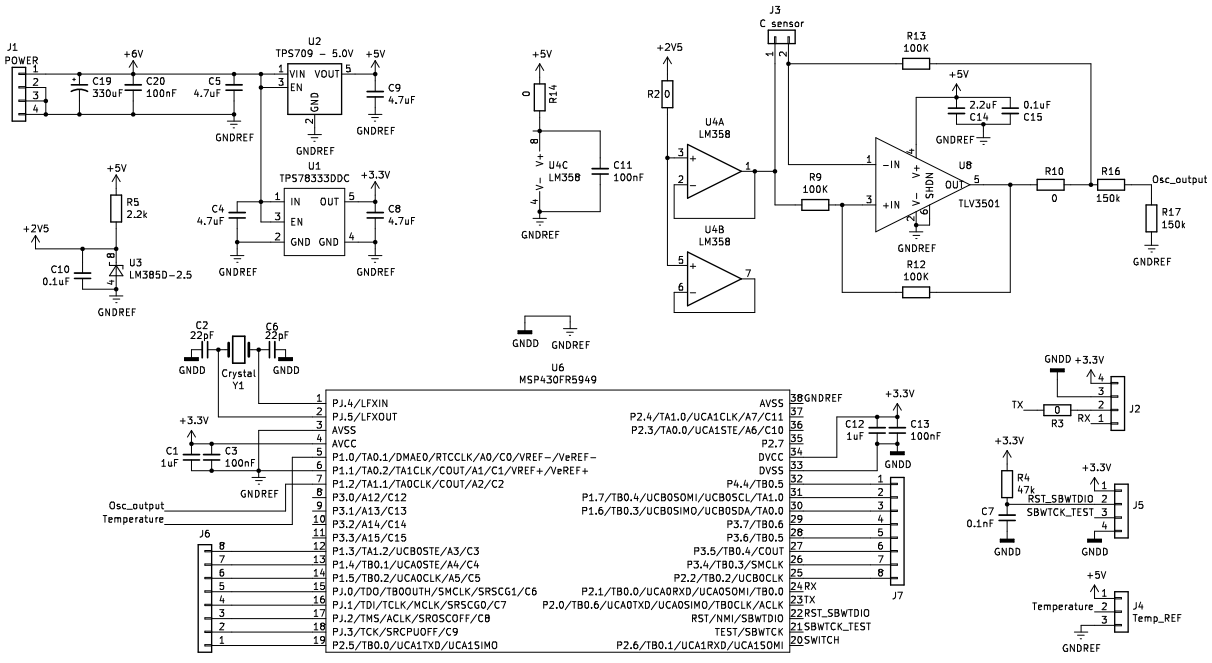

Figure 4.2 – Schematic for moisture acquisition.

A single relaxation oscillator is firstly proposed to measure this capacitance. This circuit consist of a fast (4.5 ns) rail-to-rail comparator TLV3501, an OPA192 operational amplifier, a LM285-1.2 voltage reference, resistors R_0, R_4, R_5, R_6, and the PCB fringing field capacitor C_0.

4.2.2 Processing unit

This microcontroller MSP430FR5949 has a 16-bit architecture and a complete clock system, which can operate with an external 32.768 kHz time crystal, internal digital controlled oscillator, with a maximum frequency of 16 MHz. It also has a 12-bit programmable ADC module, 64 KB of FRAM memory, 2 KB of SRAM memory, programmable communication modules and a 16-bit timer. It is powered by external source in range of 6 V to 9 V, with a 3.3 V voltage regulator.

4.2.3 Temperature measuring circuits

When driving a constant current source of $I_0 = 10\,\text{mA}$ into the copper RTD, the temperature variation of 1 °C will only result in a slight potential difference $\Delta V \approx 332\,\mu\text{V}$. Therefore, an INA 125 instrumentation amplifier is set up for providing a gain $G_V = 30.12$, so that the output of the amplifier provides a resonable slope of $dV_{out}/dT \approx 10\,m\text{V}/°\text{C}$.

A basic block diagram of the circuit is shown in Fig. 4.3, and the implemented circuit is presented in Fig. 4.4.

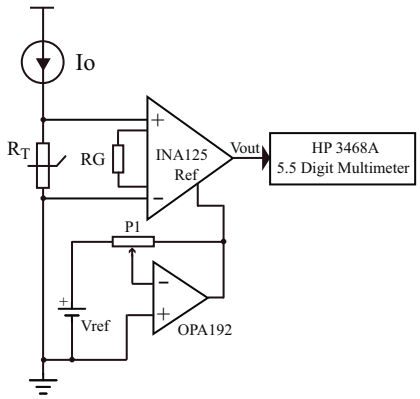

Figure 4.3 – Basic block diagram of the circuit.

The voltage at the non-inverting input of A2 appears at its inverting input due to the negative feedback, forcing the 1.2 V voltage at the LM285-1.2 to be equal to V_{R2}. Thus, the current I_0 that flows in R_2 is given by:

$$I_0 = \frac{1.2}{R_2} \tag{4.1}$$

Neglecting the base current of Q1, it can be considered that the current that enters in Q1 emitter is equal to the current that leaves its collector, going through to the copper RTD. Considering $R_2 = 1.2\,\text{k}\Omega$, the nominal value of $I_0 = 10\,\text{mA}$

The resultant voltage at the copper RTD is amplified by the INA125 (A1), in which gain is given by:

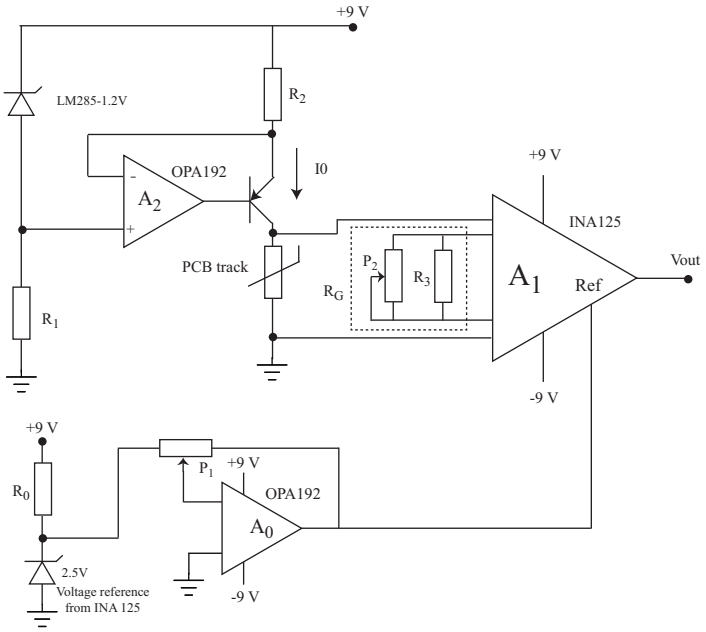

Figure 4.4 – Implemented circuit.

$$G_V = 4 + \frac{60k}{R_G} \tag{4.2}$$

The resistance R_G is the resistance equivalent of P_2 in parallel to R_1. By ajusting P_2, we can force the output voltage of A1 to have a well-defined thermal behaviour, $V_{out} = 10\,\mathrm{mV/°C}$.

Since $R_0 \neq 0$ at $T_0 = 0\,°\mathrm{C}$, there is an offset at the output of the amplifier. It was applied to the INA125 instrumentation amplifier a negative voltage generated by a second OPA192 operational amplifier (A0) configured as inverting amplifier in order to cancel this effect.

4.2.4 Moisture measuring circuit

The voltage V_{R4} is buffered by OPA192, in which creates a symmetrical hysteresis, by means of $R_6 = R_5 = 100\,\mathrm{k\Omega}$, for charge and discharge signal around $V_{dd}/2$. Assuming that the comparator could reach V_{dd} and zero, a hysteresis of $V_{dd}/4$ defines the comparator trip points at $V_{TH} = 3V_{dd}/4$ and $V_{TL} = V_{dd}/4$. The relaxation oscillator is shown in Fig. 4.5.

$$F_{osc} = \frac{1}{R_0 C_0 \ln(3)} \tag{4.3}$$

The resistor R_0 was calculated by choosing a full scale oscillating frequency $Fosc_{(FS)} \approx 22\,\mathrm{kHz}$ (period $T \approx 45\,\mu\mathrm{s}$). With this oscillating frequency, the rise and fall time of the comparator can be neglected since it is three orders of magnitude smaller

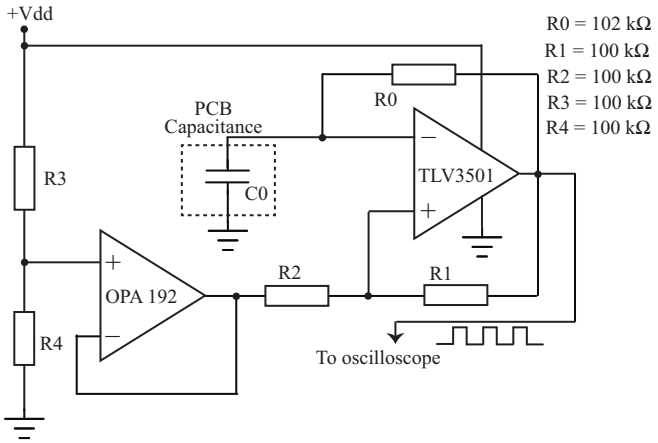

Figure 4.5 – Circuit of the relaxation oscillator.

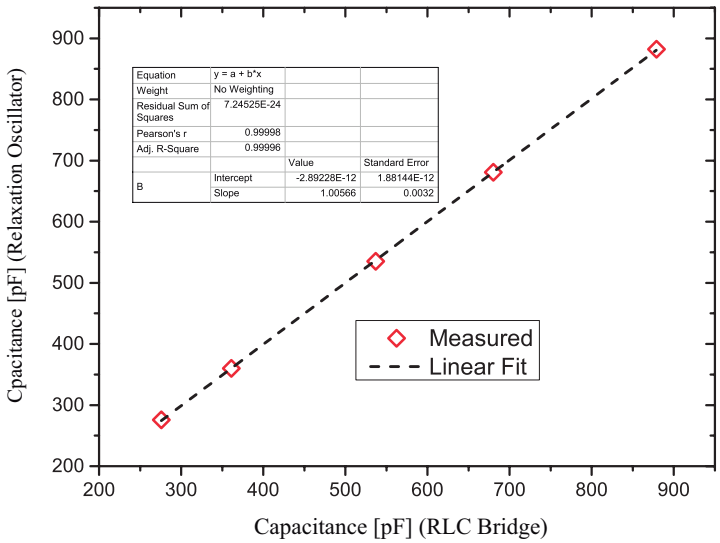

Figure 4.6 – Comparison of the capacitors measured with the Genrad 1659 RLC Digibridge and the developed relaxation oscillator.

than the period of the oscillating square wave. Therefore, the time required for cycling C_0 through a resistor R_0 between $V_{TH} = 3V_{dd}/4$ and $V_{TL} = V_{dd}/4$ is given by:

$$T_{osc} = 2\,[R_0 \ln(3)]\,C_0 \tag{4.4}$$

Rearranging the Eq. (4.3) for $C_0 \approx 400\,\text{pF}$ and $Fosc_{(FS)} \approx 22\,\text{kHz}$, we have $R_0 \approx 103\,\text{k}\Omega$, so we used $R_0 = 102\,\text{k}\Omega$.

Five commercial capacitors in the 275.5 pF to 878.4 pF range were measured by the relaxation oscillator in order to evaluate its performance. Using an oscilloscope, the measured frequency F_{osc} of each commercial capacitor was evaluated and the respective capacitance C_0 was calculated by rearranging the Eq. (4.3) as:

$$C_0 = \frac{1}{R_0 F_{osc} \ln(3)} \tag{4.5}$$

Additionally, the commercial capacitors were also measured with a Genrad 1659 RLC Digibridge. The plot shown in Fig. 4.6 presents a comparison of the capacitors measured with the RLC bridge (C_{RLC}) and with the relaxation oscillator ($C_{circuit}$). The straight-line equation can be written as:

$$C_{circuit} = 1.006\, C_{RLC} - 2.89 \times 10^{-12} \tag{4.6}$$

4.2.5 Experimental setup

Initially, a thin silicone layer was sprayed on the LM135 temperature sensor surface to protect it from water exposure, and then it was glued to the PCB sensor surface. On top of that, three pieces of an squared absorbent paper sized 3.0 cm x 3.0 cm were put on a scale, and they were wet with the same amount of water, resulting a mass of 0.13 g of each piece.

The multisensor was placed in a thermal chamber, and the pieces of moist paper were dropped one by one onto the surface of the multisensor while the output frequency of the oscillator was monitored with the oscilloscope. A photograph of the sensor with the 3 pieces of wet paper on its surface is shown in Fig. 4.7. This procedure was repeated with each piece of paper at $T = 20\,°\text{C}$ and $T = 30\,°\text{C}$. The temperature was measured with the LM135 connected to a HP 3468A digital voltmeter.

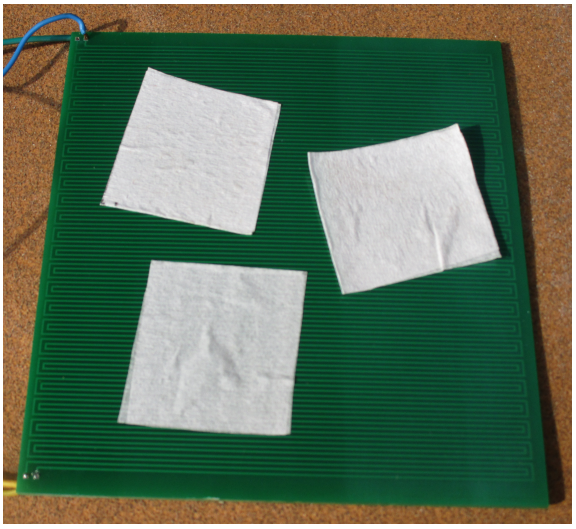

Figure 4.7 – Set-up used to measure capacitance as a function of the water mass.

4.2.6 Temperature measurements

The temperature reading comparison between the fabricated multisensor and the LM135, shown in Fig. 4.8, can be written as:

$$V_{out} = 9.956\,.T + 2.280 \tag{4.7}$$

Futhermore, the reading errors between the measured values V_{out} and the temperature T determined from the linear fit shown in Fig. 4.8 are presented in Table 4.1, considering $dV_{out}/dT \approx 10\,\text{mV/°C}$.

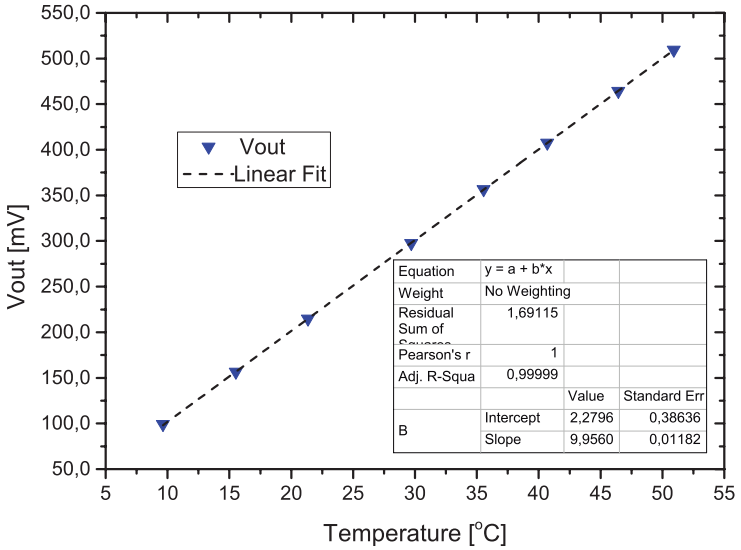

Figure 4.8 – Measured temperature with the LM135 sensor and the value of V_{out} fabricated PCB sensor.

From Table 4.1, the error E between measured values of the LM135 and the fabricated multisensor is $E \leq 0.14\,°\text{C}$. It is worth noting from previous data that the gain of the instrumentation amplifier was not precisely set (9.956 mV/°C over 10.0 mV/°C) and a small adjustment in the offset - in the negative direction - would yield an even improved match between the data measured with the LM135 and the developed multisensor.

Table 4.1 – Temperature measurements

Temperature (°C)		
LM135	**PCB sensor**	**Error**
20	20.14	0.14
25	25.12	0.12
30	30.09	0.09

4.2.7 Moisture measurements

The measured capacitance as a function of the mass of water covering the PCB multisensor for $T = 20\,°\text{C}$ and $T = 30\,°\text{C}$ is presented in Fig. 4.9 and Fig. 4.10, respectively.

As expected, we observed, for the same water mass, a variation of the measured capacitance depending on the sensor temperature. Also, both curves have approximately the same slope. The two straight lines equations from Fig. 4.11 are:

$$C = 0.147 + 2.03Mass, \tag{4.8}$$

$$C = 0.484 + 1.97Mass, \tag{4.9}$$

where the variable $Mass$ is the mass of water (in grams) and the capacitance C is given in nF.

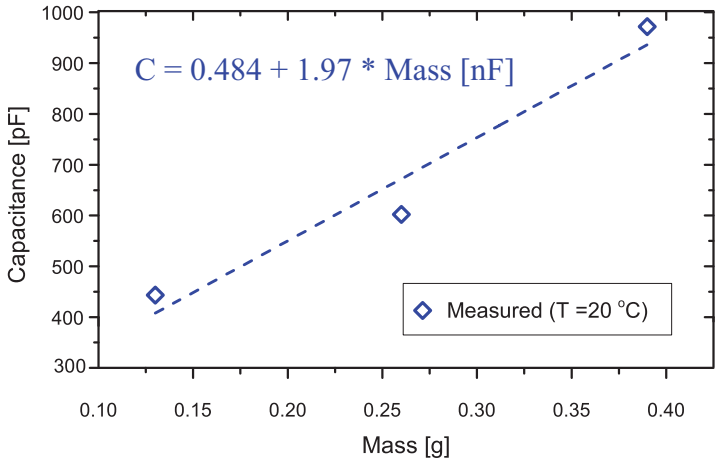

Figure 4.9 – Measured capacitance at $T = 20\,°C$

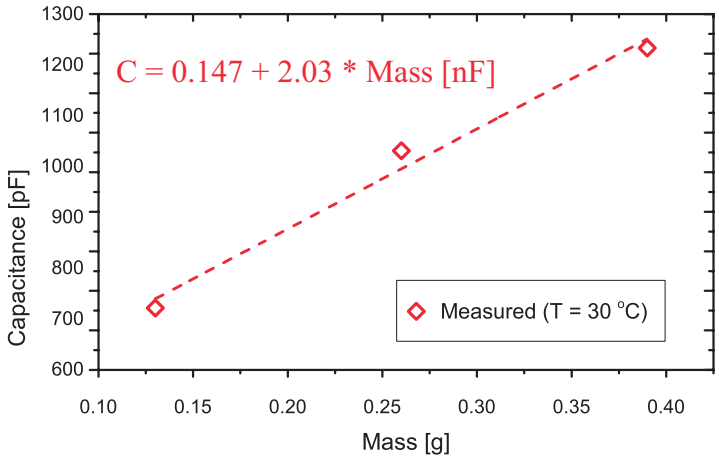

Figure 4.10 – Measured capacitance at $T = 30\,°C$

4.2.8 Temperature compensation analyses

As mentioned earlier, Fig. 4.9 and Fig. 4.10 presents a difference of the measured capacitance depending on the PCB multisensor temperature for the same water mass. Additionally, both curves present approximately the same slope, implying that the capacitance varies linearly as a function of the mass. Fig. 4.11 presents both curves plotted together.

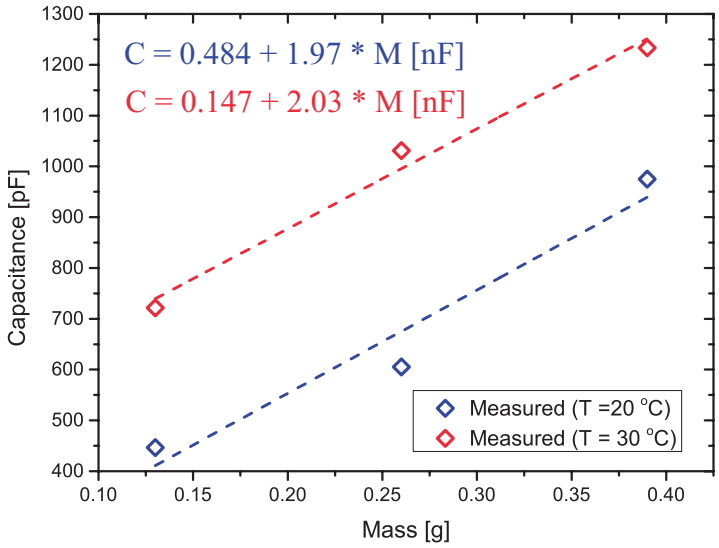

Figure 4.11 – Measured capacitance as a function of the constant water mass over two different temperatures

Due to the consideration of Eq. (4.8) and Eq. (4.9) having approximately the same slope, an average slope value of $Mass = 2nF/g$ can be used to obtain a set of equations comprising all parallel straight lines between these equations, having k as parameter:

$$C = k + 2.0Mass \tag{4.10}$$

Once there are two points (k, T) from measurement of $T = 20\,°\text{C}$ and $T = 30\,°\text{C}$, resulting $(0.484, 20)$ and $(0.147, 30)$, the value of k can be written as:

$$k = -0.527 + 0.0337T \tag{4.11}$$

Thus, it becomes possible to correct the capacitance measurements depending on the measured temperature, and obtain a reliable estimation of the water content on the PCB surface. Combining Eq. (4.5), Eq. (4.10) and Eq. (4.11), we can write:

$$Mass = \frac{1}{2}\left[\frac{1}{R_0 F_{osc}\ln(3)} + 0.527 - 0.0337T\right] \tag{4.12}$$

Although in this work we have equations to correct for the capacitance only between $T = 20\,°\text{C}$ to $T = 30\,°\text{C}$, it is straight forward to derive the equations for calculating the correct capacitance values for any temperature given that the circuit is properly calibrated.

4.2.9 Partial conclusion

A reconfigurable PCB sensor based on a modified structure of a fringing field capacitor was presented and evaluated for temperature and moisture content measurements. Using this structure it is possible to measure both capacitance and temperature.

Since both the capacitance and the dielectric constant of water changes with temperature, the proposed multisensor presents an advantage of a copper RTD sensor operating on the same substrate of the fringing field capacitor. This intrinsic characteristic of the proposed sensor provides the evaluation of compensation methods to obtain a better estimation of the moisture using the equations presented.

Moreover, it was demonstrated that measuring PCB fringing field capacitance is easily done with a simple relaxation oscillator. The circuit was well characterized by analysing its response for commercial capacitors in comparison to the same capacitors with a commercial RLC bridge. The fit line of the measured capacitance, in the 275.5 pF to 878.4 pF range presented $R^2 = 0.9994$, exhibiting a good agreement between the readings.

Since just a conventional FR-4 PCB is required to fabricate the multisensor structure, a smart-sensor comprising the multisensor itself, signal processing circuits, and a microcontroller (with an A/D converter) can be designed to measure frequency (capacitance) and the resistance of the copper tracks (temperature) at low cost. Thus, a complete low-cost moisture sensor system can be easily implemented using the reconfigurable PCB sensor presented.

4.3 A Reconfigurable Multisensor for Measuring Temperature and Moisture in Stored Grains

This section is partially reproduced from the paper "A Reconfigurable Multisensor Based on Printed Circuit Board Technology for Measuring Moisture Content and Temperature in Stored Grain",Published in: IEEE Transactions on Instrumentation and Measurement. (2022) 71, 9506110. ©2022 IEEE, doi:10.1109/TIM.2022.3170979

The multisensor was designed through four-layer FR-4 PCB with a protective conventional polymeric solder mask. The sensing area is located at the bottom and the signal processing circuits on the top of PCB, as shown in a photograph of the fabricated sensor presented in Fig. 4.12.

4.3.1 Signal processing circuits

As presented in Chapter 3, RTDs produces small $dR(T)/dT$ and bridge circuits are an attractive alternative to accurately measure the small resistance changes [64].

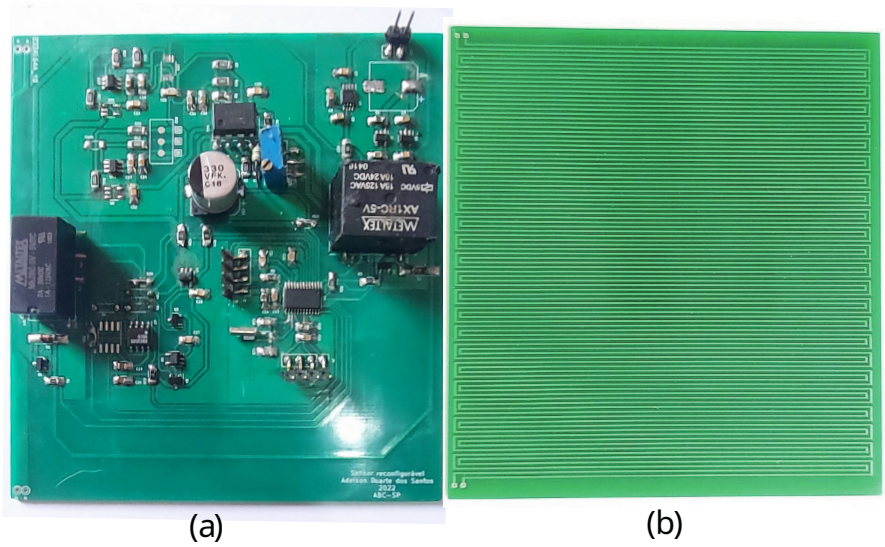

Figure 4.12 – Photograph of the PCB sensor with the signal processing circuits. (a) Top side, with the components soldered. (b) Bottom side, with the reconfigurable sensor.

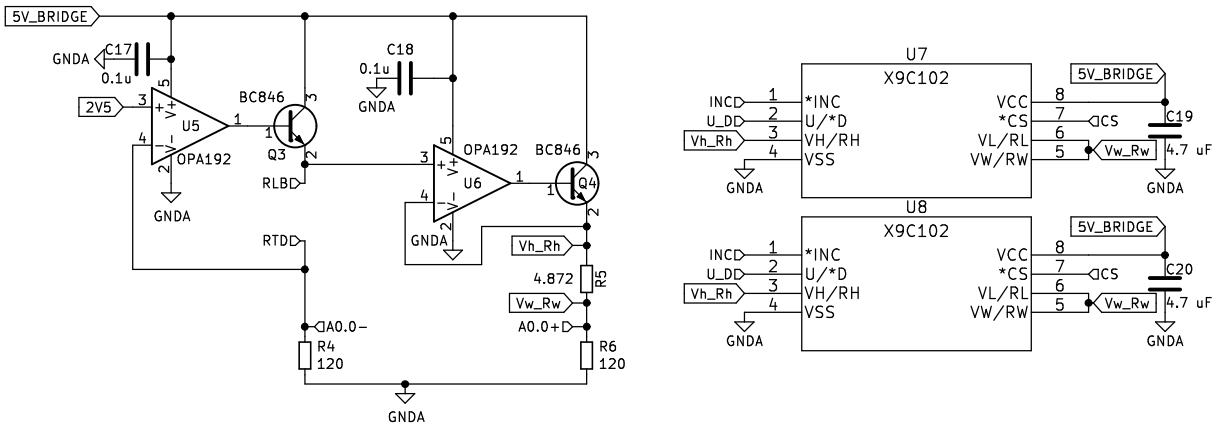

Figure 4.13 – New schematic for temperature acquisition.

The schematic for temperature acquisition is shown in Fig. 4.13. The voltage proportional to the temperature was acquired using a modified bridge topology, where a constant current is applied to one arm, and the voltage on this branch is transferred to the other bridge arm. The main characteristic of this approach is the independent adjustment of the gain and the offset in the temperature signal, allowing an easy calibration.

The output signal from relaxation oscillator circuit described in Chapter 3 has been upgraded to explore the high resolution acquisition of an A/D converter of the MSP430AFE232 microcontroller and to enable a ratiometric measurement of the capacitance. The schematic for moisture acquisition is shown in Fig. 4.14.

Lately, the schematics of other important blocks such as microcontroller, switches and power management are presented in Fig. 4.15.

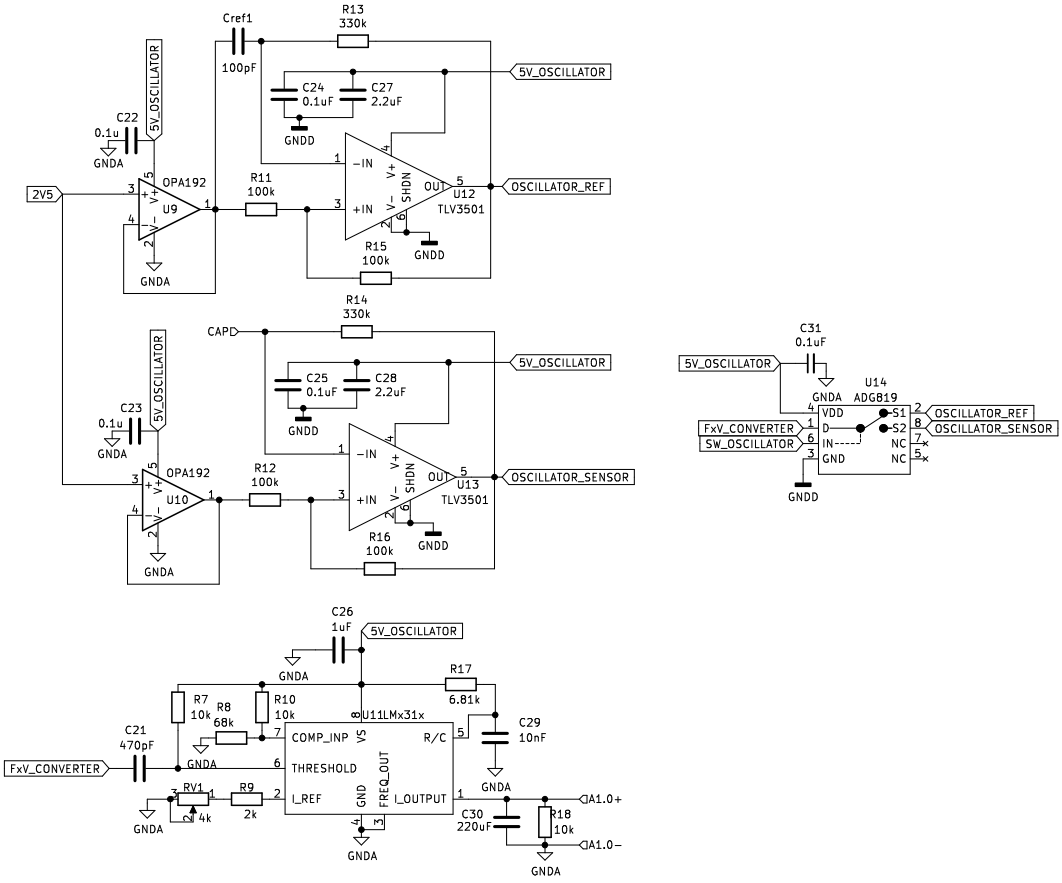

Figure 4.14 – New schematic for moisture acquisition.

4.3.1.1 Temperature Measuring Circuit

Typically exposed to high thermal amplitudes and solar radiation, aeration techniques are employed to control the temperature variation within the silo. Generally, the temperature must be kept in the $10\,°C \leq T \leq 25\,°C$ range to slow mold growth and inhibit insect activity.

The temperature was evaluated using $R(T)$ values in the $0\,°C \leq T \leq 40\,°C$ range. The larger temperature range also provides more information from the behaviour of the copper RTD design.

Bridge circuits may be driven by constant voltage or constant current, as shown in Fig. 4.16(a), Fig. 4.16(b) and Fig. 4.16(c). Configurations of Fig. 4.16(a) and Fig. 4.16(b) present some nonlinearity in the differential output voltage V_0 when a single-element varying resistor is used, respectively, given by:

$$V_0 = \frac{R}{2R + dR} V_{bias} \tag{4.13}$$

$$V_0 = \frac{R}{2R} V_{bias} \tag{4.14}$$

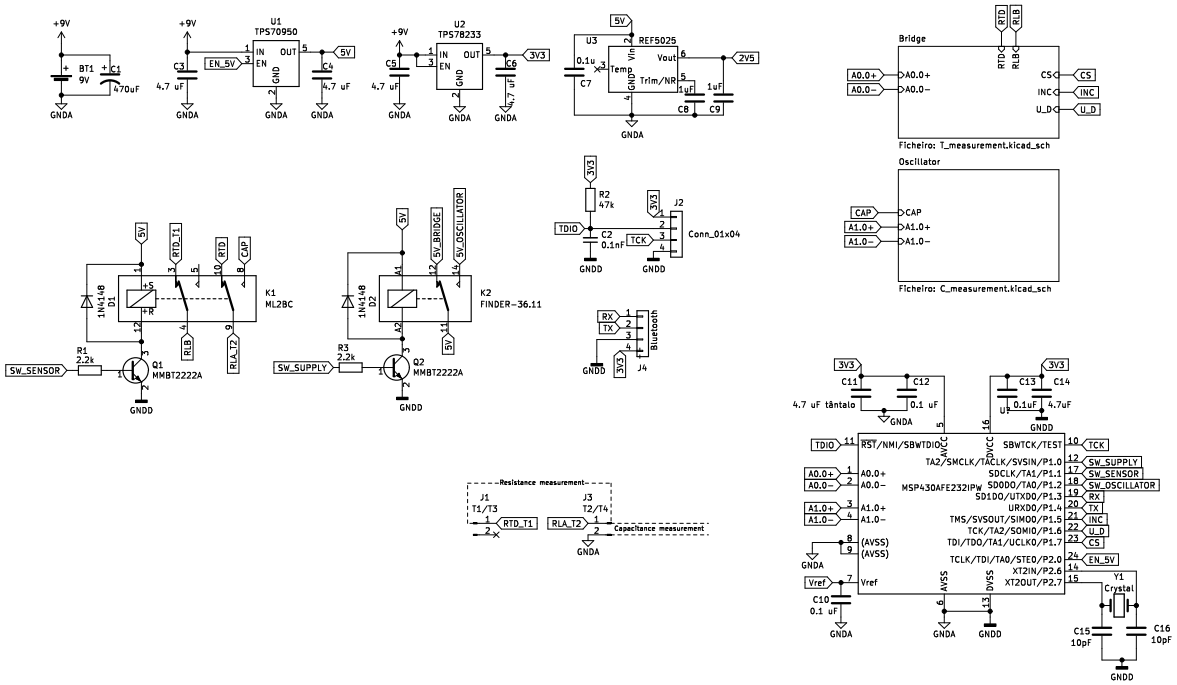

Figure 4.15 – Schematic of power supply, switches and the microcontroller for the prototype.

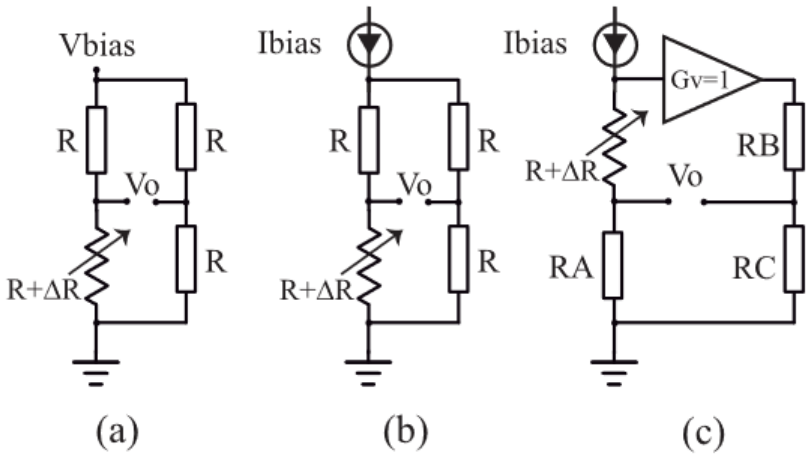

Figure 4.16 – Bridge circuits [34]. (a) Voltage driven bridge. (b) Current driven bridge. (c) Modified bridge circuit.

The simplified schematic based on the modified topology (Fig.4.16(c)) is shown in Fig. 4.17. On the left branch, the current source I_0 comprises the OPA192 operational amplifier (A1), a bipolar transistor (Q1), a bandgap voltage reference V_{REF}, a low TC resistor R_{REF}, and the RTD resistance R_T. Through negative feedback, the potential V_{REF} applied to positive input of (A1) is forced on the center of the bridge, resulting $V_1 = V_{REF}$. The current that flows in R_{REF} is given by:

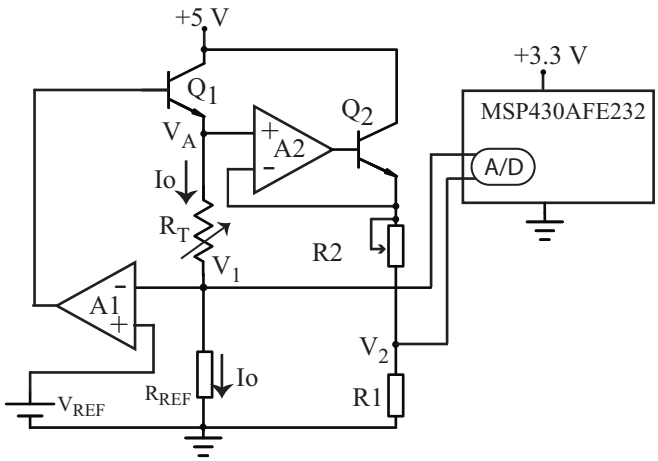

Figure 4.17 – Simplified implemented bridge circuit [34].

$$I_0 = \frac{V_{REF}}{R_{REF}} \tag{4.15}$$

The bandgap voltage reference REF5025 (TI) has initial voltage accuracy $V_{REF} = 2.5\,\text{V} \pm 0.05\,\%$, $3\,\text{ppm/°C}$ maximum temperature drift and very-low noise, $3\,\mu\text{Vpp/V}$. The OPA2192 has low input offset voltage $V_{os} = \pm 5\,\mu\text{V}$, low input bias current $I_{bias} \approx \pm 4\,\text{pA}$, and a very low drift $dV_{os}/dT = \pm 0.1\,\mu\text{V/°C}$. These components were selected in order to minimize the influence of temperature over the measurements and to provide a well defined and constant current source I_0.

The voltage in the emitter of (Q1), V_A is given by:

$$V_A\,(R_T) = V_{REF} + I_0 R_T, \tag{4.16}$$

and is composed of a constant term (V_{REF}) and a term that varies with temperature ($V_{RT} = I_0 R_T$).

At the top of the left branch, the voltage V_A is sent to a second OPA192 operational amplifier (A2), in which is connected as a follower with a bipolar transistor (Q2) as a current buffer. The top right branch of the bridge is driven by (Q2) and this branch is a simple voltage divider, composed by R_2 and R_1. If neglecting the I_{bias} of (A1) and (A2) the current I_0 will flow just through the RTD R_T. Choosing a drive current $I_0 = 20\,\text{mA}$, the input bias current can be neglected compared to I_0.

For $T = 0\,°\text{C} \rightarrow R_T = R_0$, and the bridge must be perfectly balanced. Choosing $R_1 = R_{REF}$ it forces $R_2 = R_0$, it results in voltage divider output (V_2) following the voltage variation on the RTD (V_{RT}) given by:

$$V_2 = V_A \frac{R_1}{R_1 + R_2} \rightarrow V_2 = V_A \frac{R_1}{R_1 + R_0} \tag{4.17}$$

Using Eq. (4.17), we we can write the output of the bridge ($V_d = V_2 - V_1$) as:

$$V_d = V_2 - V_1 \rightarrow V_d = V_A \frac{R_1}{R_1 + R_0} - V_{ref} \tag{4.18}$$

The voltage $V_d = V_2 - V_1$ is sent to one of the internal differential input A/D converters of the microcontroller MSP430AFE232 and is multiplied with a gain G_V to provide a signal with the desired output scale. The output voltage calculated by the microcontroller is:

$$V_{out} = G_v V_d \tag{4.19}$$

The characteristic of R_T as a function of the temperature is an intrinsic property of the PCB copper tracks and must be measured. After we measure this characteristic of $R_T(T)$, we obtain R_0 and dV_{RT}/dT.

4.3.1.2 Capacitance measuring circuit

It was added to the relaxation oscillator circuit a frequency-to-voltage converter (FxV) using a LM231 (TI). Ideally suited for use in precision frequency-to-voltage conversion of simple low-cost circuits, the LM231 presents a full scale frequency of 10 kHz and, $\pm 0.06\,\%$ non-linearity. Its output is filtered and read by a second internal A/D converter of the MSP430AFE232 microcontroller. The complete capacitive measuring circuit is shown in Fig. 4.18.

As observed in Fig. 4.18, a second identical relaxation oscillator circuit is added but with a known capacitor C_{REF} in lieu of the sensor capacitance C_0. The frequency of this oscillator will be:

$$F_{REF} = \frac{1}{2\left[R_0 \ln(3)\right] C_{REF}} \tag{4.20}$$

Thus, using Eq. (4.3) and Eq. (4.20) for $F_{osc} = F_{sensor}$ we can write

$$C_{sensor} = C_{REF} \frac{F_{REF}}{F_{sensor}} \tag{4.21}$$

Through an analog switch ADG819 (Analog Devices), the LM231 can receive alternately the output voltages of both oscillators. The ADG819 is a CMOS, single-pole, double-throw (SPDT) switch with very low resistance $R_{on} = 0.5\Omega$. Therefore, the output voltages for each oscillators are given, respectively, by:

$$V_{out(sensor)} = kF_{sensor} \tag{4.22}$$

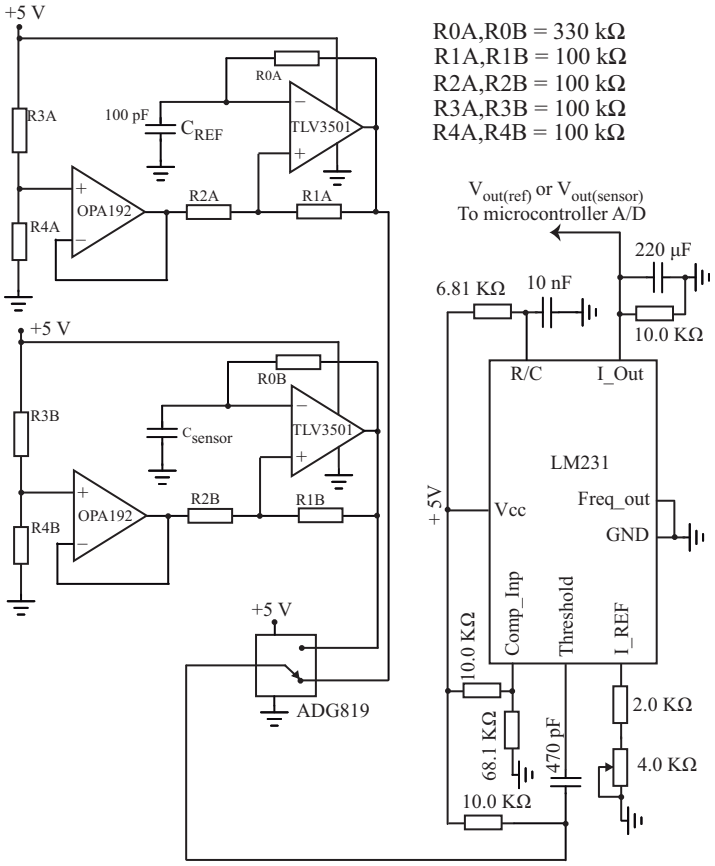

Figure 4.18 – Complete capacitive measurement circuit [34].

$$V_{out(REF)} = kF_{REF} \tag{4.23}$$

Replacing Eq. (4.22) and Eq. (4.23) into Eq. (4.21), C_{sensor} can be written as:

$$C_{sensor} = \left(\frac{V_{out(REF)}}{V_{out(sensor)}} \right) C_{REF} \tag{4.24}$$

Due to the large time constant of the LM231 output filter, the microcontroller waited 30 seconds before making the A/D conversion in each oscillator.

4.3.1.3 Sensor reconfiguration on-the-fly

The copper tracks of the PCB must be connected to different circuits, depending on what is being measured: capacitance or temperature. The simplified circuit diagram presented in Fig. 4.19 shows how the sensor was reconfigured, on-the-fly, to make the two distinct measurements.

A DPDT PCB relay (ML2BC1, from Metaltex, Brazil) was used to reconfigure the sensor. Firstly the relay was used to connect the contacts T1 and T2 of one of the continuous copper tracks to the contacts RTD with RLB and RLA, respectively. This connection allowed for the temperature measurement. At the same time, another relay

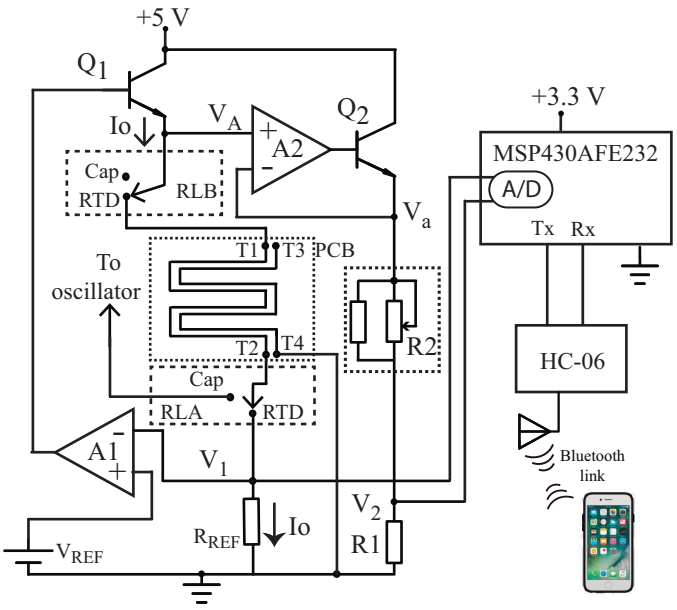

Figure 4.19 – Sensor reconfiguration is made with a DPDT miniature relay (RLA and RLB) [34].

(not shown in the simplified diagram of Fig. 8) turned on the 5 V power supply of the analog part of the circuit and shut down the power of the oscillator circuit.

Next, after the temperature measurement was finished, the 5 V analog circuit power supply was shut down and the 5 V oscillator circuit was turned on. The contact T1 of the copper track was left floating (using RLB) and contact T2 was connected (with RLA) to the oscillator circuit. This configuration allowed for a capacitance measurement. Copper track contacts T3 and T4 are permanently floating and connected to the ground, respectively.

4.3.2 Experimental setup

The multisensor was fabricated at JLCPCB, one of China's largest PCB prototype manufacturer. Considering that a new sensing structure has been built, its further characterization is required and it will be described in the following paragraphs.

4.3.3 Sensor characterization

A resistance characterization over temperature was performed with the sensor within in a thermal chamber. The temperature range of $10\,°C \leq T \leq 50\,°C$ was evaluated with a LM135 temperature sensor used to track the temperature in the chamber. The plot of the measured resistance and the LM135 temperature sensor is shown in Fig. 4.20. The results in this small temperature range showed a very high linearity, even though the copper used to fabricate the PCB tracks was not optimized for use as an RTD.

From Fig. 4.20, $dR_T/dT = 21.07 \times 10^{-3}\,\Omega/°C$ and $R_0 = 4.847\,\Omega$, therefore:

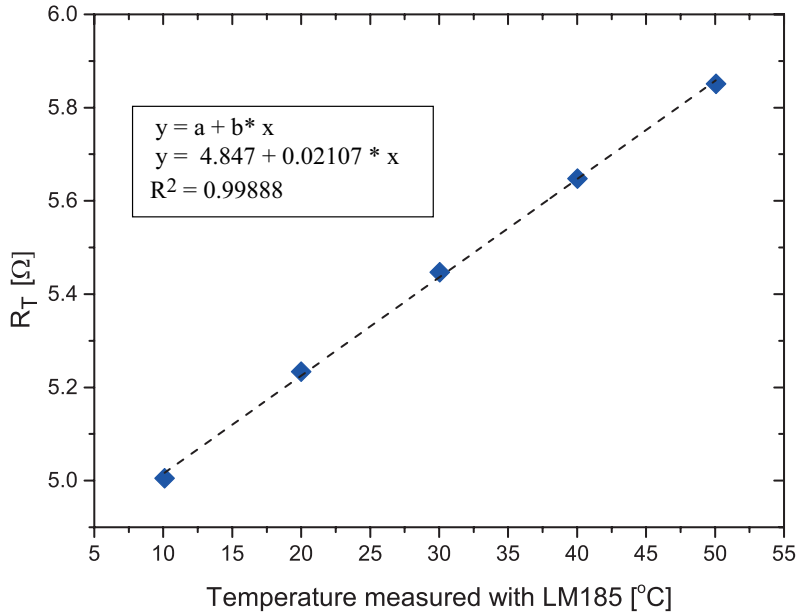

Figure 4.20 – Comparison of the temperature measured with the developed sensor and a LM135 [34].

$$R_T(T) = 4.847 + 21.07 \times 10^{-3} T \tag{4.25}$$

This equation is used to calculate the values of $R(T)$ during the bridge characterization.

4.3.4 Temperature measurements

While using a constant current source of I_0 for biasing the cooper RTD, the power dissipated in it is $P_{dissipated} \approx 1.8\,\text{mW}$, far lower than a typical value of a platinum RTD-100 ($P_{dissipated} = 100\,\text{mW}$). The bias current figure is critically relevant to the measurement, since the power dissipated in the RTD can be a source of error due to its self-heating.

The circuit was calibrated using the zero and the full-scale point (the calibration description is presented in the following subsection), so one method to evaluate the errors in the measured points is end-points nonlinearity. The Fig. 4.21 presents the results from the temperature measurements. The measured intermediate points showed a maximum end-points nonlinearity of $\mid E_{nl} \mid = 0.64\,^{\circ}\text{C}$, at $T = 16.5\,^{\circ}\text{C}$.

4.3.4.1 Calibration of the bridge circuit

The modified bridge circuit implemented in this thesis has the advantage to provide an independent gain and offset adjustment. In order to exploit this intrinsic characteristic of this bridge circuit, a self-calibration technique is employed on the offset of the circuit by means of a feedback loop. Using a digital potentiometer (X9C102, from

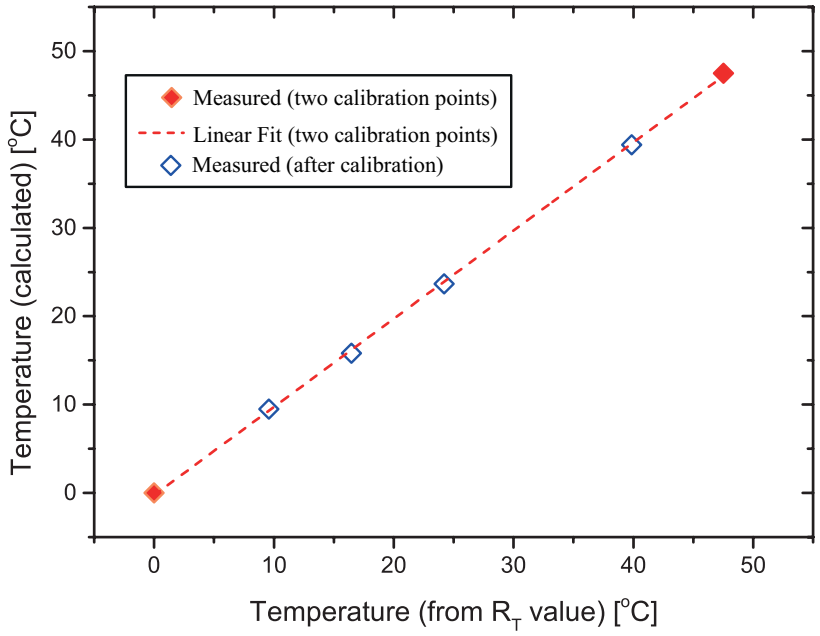

Figure 4.21 – Measured V_{out} as a function of the temperature (calculated with R_T values) [34].

Xicor, Inc., USA) on the upper right branch of the bridge interfacing a microcontroller, a calibration similar to any circuit with RTDs was accomplished in simple steps:

(1) the circuit was turned on and an internal routine in the microcontroller zeroed the offset of the A/D converter;

(2) Next, a trimmed resistor was adjusted until its value was equal to the resistance of the PCB track at 0 °C (R_0) and connected to the contacts of the RTD in the circuit;

(3) With this resistor connected, the microcontroller A/D converter performed a conversion, reading the value of V_d;

(4) If V_d was not zero (when perfectly balanced, V_d must be equal to zero), the microcontroller adjustes the digital potentiometer (P2) and a new A/D conversion is performed.

Steps 3 and 4 are repeated until $V_d = 0$. It is worth noting that, at 0 °C (R_0), the digital potentiometer allowed for the zero adjustment in steps of approximately 5 μV. Since the A/D resolution operates at 36.6 μV, one can consider that a perfect zero adjustment was always obtained.

For the gain adjustment, the following steps were done:

(1) First it was chosen a dV_d/dT for this signal processing of $dV_d/dT = 10\,\text{mV}/°\text{C}$;

(2) A trimmed resistor is used in the place of the sensor and adjusted until its value was equal to the resistance of the PCB track at a higher temperature (we used 47.5 °C since seed damage occurs beyond this temperature level);

(3) The value of V_d is measured and a line equation is calculated using this point and the zero point;

(4) The slope of this line is used to calculate, inside the microcontroller, the gain G_v to obtain the correct value of $V_{out} = 475\,\text{mV}$.

4.3.4.2 Tolerance analyses

It is important to analyze how the tolerance of the components affects the performance of the bridge circuit, since this novel smart sensor will be subject to external influences. As it is a relatively simple circuit, it was decided to make corner analyses considering just the thermal variations of V_{REF}, R_{REF}, R_1, and R_2.

For investigating that, it was considered the offset adjustment made at $T = 25\,°\text{C}$, in the middle of the evaluated points of $T = 0\,°\text{C}$ and $T = 50\,°\text{C}$. Thus, the errors at the bridge output V_d were calculated at these extreme temperature points. An important aspect to keep in mind is during the calibration, $V_d = 0\,\text{V}$ is guaranteed whenever a resistor with $R_T = R_0$ is included in the sensor's position, regardless of the unmatched values of R_{REF} and R_1.

Accordingly, the corner analyses were made considering the extreme values of:

- $V_{REF} \pm \Delta V_{REF}$ @ $TC = \pm 3\,\text{ppm/°C}$;
- $R_{REF} \pm \Delta R_{REF}$ @ $TC = \pm 5\,\text{ppm/°C}$;
- $R_1 \pm \Delta R_1$ @ $TC = \pm 5\,\text{ppm/°C}$;
- $R_x \pm \Delta R_x$ @ $TC = \pm 5\,\text{ppm/°C}$;
- $X9C102$ @ $TC = \pm 600$ ppm/°C;

The resistor R_2 is composed by R_x in parallel with the digital potentiometer X9C102 (Fig. 4.19). The TC of X9102 is three orders of magnitude higher than R_x, so its thermal variations do not significantly affect the value of R_2, presenting just few mΩ of variation when X9C102 swings within its outer limits.

The worst case error found were $E_{Vd} = 53\,\text{ppm}$ and $E_{Vd} = 43\,\text{ppm}$ for $T = 0\,°\text{C}$ and $T = 50\,°\text{C}$;. This analysis shows a signal processing circuit with a degree of robustness regarding temperature influence.

4.3.5 Capacitance measurements

The signal conditioning circuit for capacitance measurements can be split into two parts: relaxation oscillator and frequency-voltage converter. The first was characterized previously and can be seen in Fig. 4.6. The latter will be presented in the following paragraphs.

4.3.5.1 Frequency-to-voltage conversion

A frequency-to-voltage converter will convert the frequency of its input into a proportional voltage in its output, as presented in Eq. (4.22). The basic circuit consist of several signal processing blocks, in which comprises a high pass network, a comparator, an integrator and a charge pumping. A simplified schematic of a frequency-to-voltage converter is presented in Fig. 4.22.

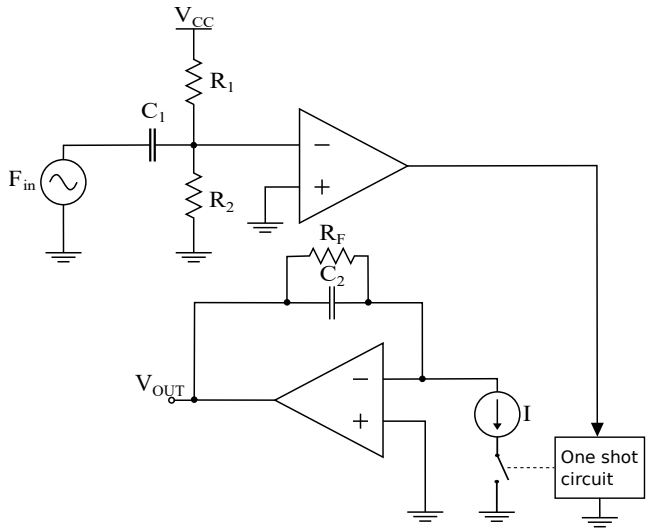

Figure 4.22 – Simplified schematic of a frequency voltage converter.

The network comprised by R_1, R_2, and C_1 is a high pass filter connected to the non inverter input of a comparator. A spike occurs at this point due to the derivative function of the filter when estimulated with squared wave. The one shot circuit is driven when a spike occurs and then the constant current source I is driven in integration block, comprised by a second operational amplifier, R_f, and C_2. Therefore, the voltage output V_{out} will be proportional to the RC constant of the integration block.

In our design (Fig. 4.18) the circuit input comprises a high pass network of R_5 and C_1, which operates as a derivative function to the input signal. For a square waveform from the relaxation oscillator, this operation causes spikes at *threshold* pin in both directions. Next, these spikes are compared to a constant voltage from a voltage divider formed by R_7 and R_6 and connected to the integrated comparator, *comp-inp* pin. At negative edges of input signal, the derivative will result in a voltage at *threshold* pin lower than the voltage at *comp-inp* pin, thus triggering an internal switch for the operation

of the internal current pump. The value of this current is defined in terms of R_9, R_{10}, and by a 1.9V from the internal band-gap reference as:

$$I_{REF} = \frac{1.9V}{R_9 + R_{10}}, \tag{4.26}$$

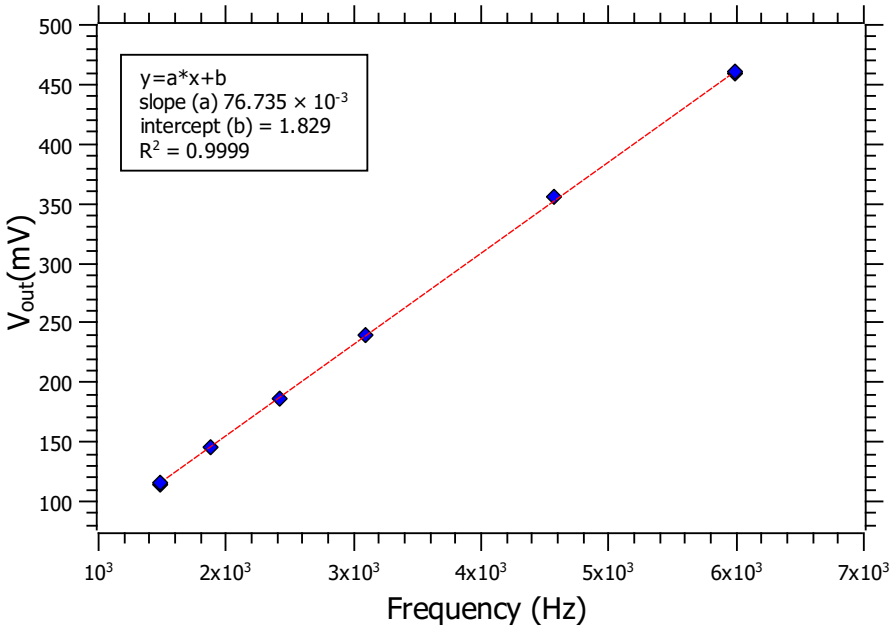

Figure 4.23 – Output voltage of the FxV converter in function of the frequency.

Finally, this current is mirrored to the output filter comprised by R_{11} and C_3 and the integration of the signal is perfomed. The integration of the signal continues until the second integrated comparator turns the internal switch OFF (thus, disabling the current source) due the time- constant defined by R_8 and C_2.

We used $R_5 = 10\,\text{k}\Omega$ and $C_1 = 470\text{pF}$ to pass frequency above 30 kHz of the squared input signal from the relaxation oscillator. This filtered signal was then compared to a 4.3 V voltage reference comprised by voltage divider $R_6 = 68.1\,\text{k}\Omega$ and $R_7 = 10\,\text{k}\Omega$. The resistors R_9 and R_{10} were adjusted using the Eq. (4.26) to 12 kΩ and 4.3 kΩ, respectively, to provide a $I_{REF} \approx 120\,\mu\text{A}$ during a period defined by $R_8 = 6.81\,\text{k}\Omega$ and $C_2 = 10\,\text{nF}$. Finally, the output filter was comprised by $R_{11} = 10\,\text{k}\Omega$ and $C_3 = 220\,\mu\text{F}$.

Additionally, this circuit was calibrated by the same method of the relaxation oscillator calibration, described in Chapter 3 - adding five commercial capacitors in the 275.5 pF to 878.4 pF - and evaluating the output voltage in function of the input frequency. The plot of circuit response is presented in Fig. 4.23.

The linear fitted equation of the FxV converter has $R^2 = 0,9999$ and can be written as:

$$V_{out} = 76.735 \times 10^{-3} F + 1.829 \tag{4.27}$$

The plot of the measured capacitance using the proposed circuit and the capacitors value measured with the GenRad Digibridge is shown in Fig. 4.24.

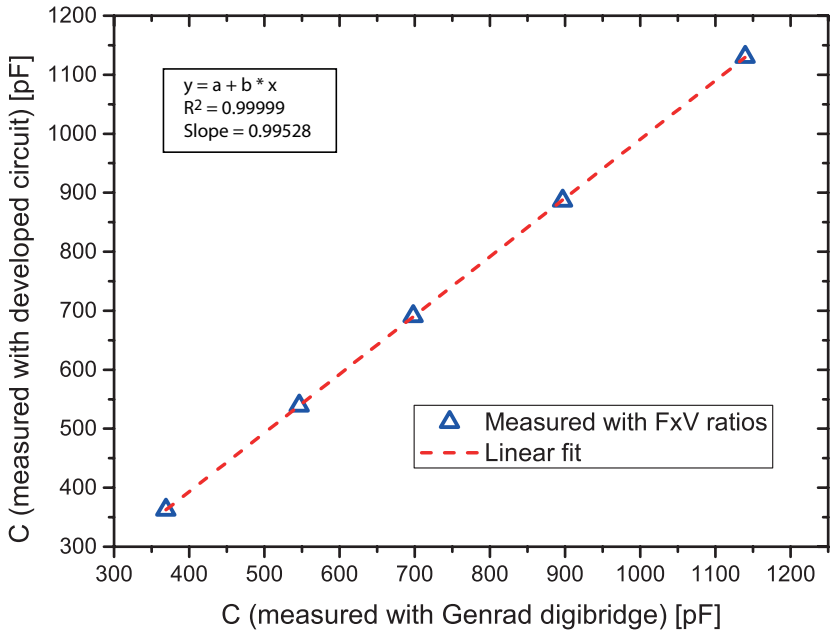

Figure 4.24 – Plot of measured capacitance with the proposed circuit as a function of their values measured with a GenRad 1659 RLC Digibridge [34].

As we can observe in Fig. 4.24, the measured circuit presented an excellent performance, as the linear fitted equation has $R^2 = 0.9999$ and a slope practically equal to 1 (S = 0.99528).

4.3.6 Moisture content measurements

The average grain MC is found to be proportional to the grain sample weight in the range of 9 % - 27 % MC, by various corn kernel samples measured with a commercial grain moisture tester (AgraTronix MT-16, USA) [19]. The corn is harvested with a MC of approximately 22 % to 25 % and must be stored in silos with a moisture in the range of 13 % - 15 %, so the multisensor was evaluated with corn kernels in the 5.2 % - 22.2 % range.

A sample of handpicked corn ears shelled by hand was used to measure the capacitance of the sensor as a function of the corn kernel weight. Initially, the corn sample was weighed (at approximately $T = 21\,°C$). Next, the sample was dried in an oven (for different periods of time), weighed, and several capacitance measurements were performed, so that different MC levels were achieved in each measurement. For each MC level, the capacitance was measured five times, with a 5-minutes interval, to check the repeatability of the sensor.

It is worth mentioning that the measurements were taken with the corn sample poured over the PCB in a horizontal position, since the non-spheric characteristic of the corn kernel potentially leads to divergent results from a vertically placed sensor [65].

Finally, following all capacitance measurements, the sample was left in the oven for 24 h, to ensure that all the water would evaporate from the grains. So based on this dry sample, the amount of water in all measurements could be precisely determined by the sample weight. The measured capacitance as a function of the percent volumetric MC, presented in Fig. 4.25, can be writen as:

$$C_{sensor} = 9.29548 \times 10^{-13}\, MC + 2.42956 \times 10^{-13} \tag{4.28}$$

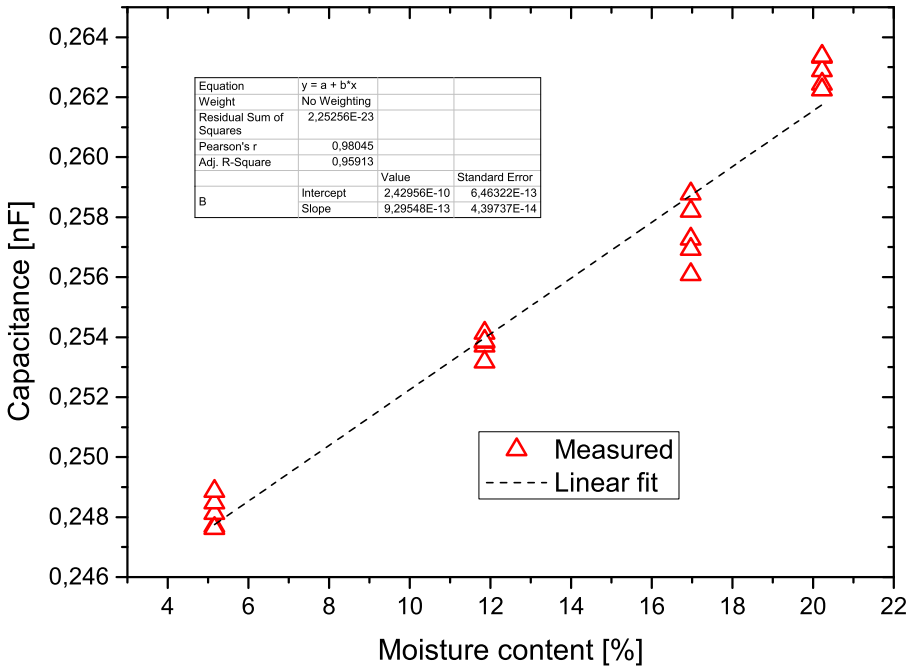

Figure 4.25 – Plot of measured sensor capacitance versus MC [34].

Additionally, Table 4.2 shows the repeatability test for capacitance measurement. The highest value of the standard deviation was found to be 1.06 pF, two orders of magnitude smaller than the mean value 257.5 pF, measured at $MC = 16.9\,\%$.

Table 4.2 – Repeatability Test [34].

MC [%]	**Mean Value [pF]**	σ **[pF]**
5.2	248.1	0.52
11.9	253.7	0.35
16.9	257.5	1.06
20.2	262.8	0.51

c

4.3.7 Processing unit

The microcontroller MSP430AFE232 is powered by an external source in range of 6 V to 9 V with a 3.3 V voltage regulator. The CPU operates at 12 MHz, as the communication peripheral, provided by a internal digitally controled oscillator and a RTC crystal of 32.768 kHz is used to an A/D converter and timer peripherals.

The TPS7A0333 and TPS70950 (Texas instruments) are low-dropout voltage regulators with ultra-low quiescent current of 200 nA and 1 μA, and presents output accuracy over temperature of 1.5 % and 2 % respectively. These were important parameters of the power management, whereas the proposed multisensor will be subject of a wide temperature gradient when inside the silo. The first voltage regulator provides 3.3 V and is dedicated to the microcontroller, the latter is dedicated to the signal processing circuits. Both regulators were connected in parallel with the external power supply, so we can easily operate the TPS70950 to provide energy savings during iddling periods.

Both analog output signals of the sensor signal processing circuits were multiplexed by the internal A/D converter and a gain of $G_V = 1$ was applied to the signals. The temperature measurements were obtained with the bipolar 15-bit resolution mode, with a full scale voltage of 600 mV and a resolution of 36.6 μV. On the other hand, moisture content measurements were obtained with the unipolar mode of 16-bit resolution, with a full scale voltage of 600 mV, yielding a resolution of 9.15 μV.

The timer was configured to precisely turn on the microcontroller each 5 minutes to get a measurement of each sensor. It also provided a settlement time of 30 seconds, the duration of the moisture content measurements. The measured data stored in the microcontroller (capacitance and temperature) were transmitted to an external device using a bluetooth link HC-06 module (Guangzhou HC Information Technology Company, China). The data were read in a smartphone, using the serial bluetooth terminal app, available at the Google Play. The microcontroller waits for a command from the serial terminal, and once it is received it, the values stored in the A/D converter are transmitted to the smartphone. The baud rate of the link was set at 115.200 bps.

4.4 Partial conclusion

A multisensor based on PCB technology that measures MC and temperature in grains stored in silos was presented. Due to its large sensing area, the proposed multisensor allows for averaging the MC of a large number of kernels. The simple reconfiguration of the sensor can be accomplished using a DPDT relay, thus switching between the voltage measurement of copper tracks as an RTD and the measurement of the frequency-dependent voltage of the fringing field capacitance.

The developed sensor is quite robust, reliable (the sensing elements are the copper tracks of the PCB) and all electronics are implemented on the same PCB of the sensor. The embedded microcontroller allows for the transmission of digital signals, so a two-wire communication protocol can be easily implemented, reducing the complexity of the cabling when many sensors are distributed inside the silo, and allowing for the implementation of precise aeration techniques.

Employing two relaxation oscillators, one as reference capacitance and one with the sensor capacitance, a time interval technique has successfully allowed a ratiometric measurement between them, owing to the linearity ratio of the relaxation oscillator frequencies being proportional to the capacitor ratio.

The capacitive sensor demonstrated an average capacitance variation of $C = 14.6\,\text{pF}$ when the MC in the kernel changed from $5.2\,\%$ to $20.22\,\%$, resulting in a sensitivity of $0.98\,\text{pF}/\%$. The measured values of $R_T\,(T)$ as a function of the temperature for this design were compared to a LM135 temperature sensor and presented a linear behavior in the $10\,^{\circ}\text{C}$ to $50\,^{\circ}\text{C}$ temperature range, with $R^2 = 0.99888$.

An easy to calibrate bridge circuit allowed the independent adjustment of the gain and the offset in the temperature signal processing circuit. The calibration was performed by an endpoint straight-line method (for $T = 0\,^{\circ}\text{C}$ and $T = 47.5\,^{\circ}\text{C}$), and the measured values in this temperature range presented a nonlinearity error of just $0.64\,^{\circ}\text{C}$ at $T = 16.5\,^{\circ}\text{C}$.

5 Conclusion

This chapter presents the major conclusions of the thesis discussing its findings and contributions. It also suggests future research directions that can provide new knowledge to the development of PCB reconfigurable multisensor systems for environmental sensors.

5.1 Conclusion

The first part of this work was dedicated to introduce an environmental multisensor based on PCB technology. We designed and fabricated a modified fringing field capacitive sensor based on FR-4 PCB to measure both capacitance and temperature. It was successfully evaluated in laboratory suggesting that the proposed multisensor could be an interesting fit to design reconfigurable smart-sensors.

The first sensor fabricated had dimensions of 96 mm x 92 mm. A commercial capacitance meter was able to provide capacitance readings of the sensor ranging from 300 pF to 800 pF in function of the water content over its surface at linear fashion. Using a simple circuit, it was also able to easily measure the temperature of the copper PCB tracks within a temperature chamber in the 9 °C to 50 °C range. Although the gain and the offset of the instrumentation amplifier were not precisely obtained, producing a slope of 9.956 mV/°C and an offset of 0.228 V, the linear fit ($R^2 = 0.99999$) suggests a good relationship of the copper PCB tracks over the temperature range.

It was shown in [58] that fringing field capacitance has second-order effects that cause disturbance to the capacitance measurement. Both the fringing field capacitances and the dielectric constant of water have a dependence over temperature. Thus, these effects were studied for $T = 20\,°C$ and $T = 30\,°C$ using constant water content samples and compensation equations have been proposed.

A relaxation oscillator was calibrated ($R^2 = 0.9994$) and used to measure the PCB fringing field capacitance under constant moisture content. Although our equations were applied just for correcting the fringing field capacitance in a limited temperature range, this method could be used to calculate the correct values of capacitance for any temperature. The linear nature of this phenomenon (capacitance in function of water content) can easily be implemented at any off-the-shell microcontrollers.

The most important contribution presented in this thesis is the design and the fabrication of a reconfigurable smart-sensor for measuring moisture content and temperature in stored grains. It comprises a 4-layer FR-4 printed circuit board that

includes the multisensor structure on the bottom of the PCB and the signal processing circuits on the other layers. The table 5.1 summarizes the sensor's characteristics in comparison with other with other PCB-based sensors for grain measurement.

Table 5.1 – PCB sensor summary

Reference	This work [34]	[19]	[49]
Phenomenon	Capacitive & resistive	Capacitive	Capacitive
Dimensions	96 mm x 92 mm	96.5 mm x 43.2 mm	6 × 137 mm x 41.5 mm
Range	248 pF$\leq C \leq$ 264 pF	89.5 pF$\leq C \leq$ 92 pF	1 pF$\leq \Delta C \leq$ 10 pF
Architecture	Reconfigurable	Not reconfigurable	Not reconfigurable
Precision	1/257 pF	1/92 pF	0.087/10 pF

Even though there are handheld instruments available with sensors that can measure MC in grain (some manufacturers are Gehaka [BR], AgroLog [DK], Shizuoka Seiki [JP]), such measuring instruments can not be placed inside silos. Also they are usually only capable of measuring very small samples of grains due to their small sensing area. The reconfigurable smart sensor has been fabricated with a large area (96 mm x 92 mm) on the robust FR-4 substrate and has many other advantages that are not found in the previously mentioned works, such as:

1 reliability: the sensing elements are the copper tracks of the PCB with a protective solder mask;

2 integration: all signal processing circuits can be implemented on the same PCB of the sensor including the processing unit;

3 infrastructure: reduction of the complexity of the cabling inside the silo using a two-wire communication protocol (e.g. RS-485);

4 cost: at present, printed circuit boards are cheap, so tens of sensors can be installed providing an accurate MC and a temperature profile of the silo;

5 real-time: reconfiguration is performed on-the-fly.

The copper RTD sensor exhibited a very linear behavior ($R^2 = 0.99888$) over the temperature range that includes the safe grain storage temperatures. The modified bridge circuit enabled a linear behavior of the differential output and eased its calibration. Furthermore, it yielded a robust measurement circuit with nonlinearity less than 0.64 °C and differential output errors of tens of ppm for both ends of the temperature range.

Corn kernels with MC percentage in the range of $MC = 8\,\%$ to $MC = 32\,\%$ were successfully measured by means of the ratiometric measurement from two identical relaxation oscillators and a frequency-to-voltage converter. When compared to the state

of the art of the fringing field capacitive sensors for grain monitoring presented by Dean et al [19], which has obtained a standard deviation of 1 part in 90 for $9\,\% \leq MC \leq 27\,\%$, the developed sensor presented a smaller standard deviation of 1 part in 257. However, differents methods were employed:

1 the repeatability test of this work was accomplished by not removing the sensor from its position in the corn kernel sample and a 5-minute interval between measurements was performed;

2 a reproducibility test presented by Dean et al. [19] was accomplished by inserting and removing the sensor from the corn sample for each measurement;

In a silo, the method 1 would be the typical setting, hence a similar standard deviation to that presented in this work should be expected.

A third source of error that is difficult to compensate and was not mentioned earlier, is that kernels are a living organism and its dielectric constant depends on its chemical composition [66]. Therefore, it is recommended that a calibration procedure with the specific kernel that will be monitored be performed at different temperatures and with different MCs. Since the proposed sensor can measure the temperature, it is easy to obtain a calibration curve of a specific kernel MC as a function of the measured capacitance and temperature.

5.2 Future research

In our work, we observed that an integrated, cost-effective and reconfigurable moisture and temperature sensor can provide insights for future decision-making algorithms developed at the edge or in the cloud for different industries.

Conducted study of data fusion algorithms to extract insights from the measur- and would improve the decision-making capability of customers and automatic industrial process. Hopefully, these algorithms can be embedded into the device, also called edge computing, thereby providing a detailed description of the observed phenomenon.

Moreover, the developed smart multisensor has not been evaluated in the field yet, therefore, we expect to characterize the sensing element in different environments, such as in soil, in a saline setting and on a weather station.

Bibliography

[1] OECD and Food and Agriculture Organization of the United Nations, *OECD-FAO Agricultural Outlook 2022-2031*. OECD-FAO Agricultural Outlook, OECD, June 2022.

[2] T. C. d. Menezes and C. J. C. Bacha, "Mudanças nos destinos das exportações brasileiras de carne bovina," *Revista de Política Agrícola*, vol. 29, no. 2, p. 50, 2020.

[3] FAO, ed., *Building a common vision for sustainable food and agriculture: principles and approaches*. Rome: Food and Agriculture Organization of the United Nations, 2014.

[4] M. Kummu, H. De Moel, M. Porkka, S. Siebert, O. Varis, and P. J. Ward, "Lost food, wasted resources: Global food supply chain losses and their impacts on freshwater, cropland, and fertiliser use," *Science of the total environment*, vol. 438, pp. 477–489, 2012.

[5] W. E. Bendinelli, C. T. Su, T. G. Péra, and J. V. Caixeta Filho, "What are the main factors that determine post-harvest losses of grains?," *Sustainable Production and Consumption*, vol. 21, pp. 228–238, Jan. 2020.

[6] C. Warrick, "Aerating Stored Grain: Cooling or drying for quality control - A Grains Industry Guide,"

[7] C. K. Ho, A. Robinson, D. R. Miller, and M. J. Davis, "Overview of sensors and needs for environmental monitoring," *Sensors*, vol. 5, no. 1, pp. 4–37, 2005.

[8] É. Lutz and P. C. Coradi, "Applications of new technologies for monitoring and predicting grains quality stored: Sensors, internet of things, and artificial intelligence," *Measurement*, vol. 188, p. 110609, 2022.

[9] I. S. o. P. Agriculture, "Precision ag definition: International society of precision agriculture." Accessed: 2023-07.

[10] C. R. Kagan, D. P. Arnold, D. J. Cappelleri, C. M. Keske, and K. T. Turner, "Special report: The Internet of Things for Precision Agriculture (IoT4Ag)," *Computers and Electronics in Agriculture*, vol. 196, p. 106742, May 2022.

[11] D. L. Hall and J. Llinas, "An introduction to multisensor data fusion," *Proceedings of the IEEE*, vol. 85, no. 1, pp. 6–23, 1997.

[12] Z. Liu, G. Xiao, H. Liu, and H. Wei, "Multi-sensor measurement and data fusion," *IEEE Instrumentation & Measurement Magazine*, vol. 25, no. 1, pp. 28–36, 2022.

[13] D. E. Moshou and X. E. Pantazi, "Data fusion and its applications in agriculture," in *Information and Communication Technologies for Agriculture—Theme II: Data*, pp. 17–40, Springer, 2022.

[14] A. B. Torres, A. R. da Rocha, T. L. C. da Silva, J. N. de Souza, and R. S. Gondim, "Multilevel data fusion for the internet of things in smart agriculture," *Computers and Electronics in Agriculture*, vol. 171, p. 105309, 2020.

[15] B. B. Sinha and R. Dhanalakshmi, "Recent advancements and challenges of internet of things in smart agriculture: A survey," *Future Generation Computer Systems*, vol. 126, pp. 169–184, 2022.

[16] T. E. o. E. Britannica, "printed circuit definition." Accessed: 2023-07.

[17] C. F. Coombs Jr, *Printed circuits handbook*. McGraw-Hill Companies, 2016.

[18] T. Syrový, R. Vik, S. Pretl, L. Syrová, J. Čengery, A. Hamáček, L. Kubáč, and L. Menšík, "Fully Printed Disposable IoT Soil Moisture Sensors for Precision Agriculture," *Chemosensors*, vol. 8, p. 125, Dec. 2020. Number: 4 Publisher: Multidisciplinary Digital Publishing Institute.

[19] R. N. Dean, J. D. Craven, E. A. Guertal, and K. A. Varnavas, "A PCB Sensor for Status Monitoring of Stored Food Stocks," *IEEE Sensors Letters*, vol. 3, pp. 1–4, Apr. 2019.

[20] O. Flor, H. Palacios, F. Suárez, K. Salazar, L. Reyes, M. González, and K. Jiménez, "New Sensing Technologies for Grain Moisture," *Agriculture*, vol. 12, p. 386, Mar. 2022.

[21] U. Ahmed, M. Kumar, B. Mahajan, M. Alam, *et al.*, "Grain moisture measuring techniques-a review," *Agricultural Engineering Today*, vol. 39, no. 2, pp. 18–24, 2015.

[22] E. Scholz, *Karl Fischer titration: determination of water*. Springer Science & Business Media, 2012.

[23] J. C. M. Diaz, "Sensor re-configurable para medidas de temperatura y humedad," 2020.

[24] L. J. Briggs, "An electrical resistance method for the rapid determination of the moisture content of grain," *Science*, vol. 28, no. 727, pp. 810–813, 1908.

[25] F. Morais, P. Carvalhaes-Dias, L. Duarte, E. Costa, A. Ferreira, and J. S. Dias, "Fringing Field Capacitive Smart Sensor Based on PCB Technology for Measuring Water Content in Paper Pulp," *Journal of Sensors*, vol. 2020, pp. 1–13, Mar. 2020.

[26] S. O. Nelson and S. Trabelsi, "Principles for microwave moisture and density measurement in grain and seed," *Journal of Microwave Power and Electromagnetic Energy*, vol. 39, no. 2, pp. 107–117, 2004.

[27] I. D. Aristizábal-Torres, "La resonancia magnética y sus aplicaciones en la agroindustria, una revisión.," *Revista Facultad Nacional de Agronomía Medellín*, 2007.

[28] R. R. Ruan and P. L. Chen, *Water in foods and biological materials*. CRC Press, 1997.

[29] C. Zhang, Z. Shi, H. Yang, X. Zhou, Z. Wu, and D. S. Jayas, "A novel, portable and fast moisture content measuring method for grains based on an ultra-wideband (uwb) radar module and the mode matching method," *Sensors*, vol. 19, no. 19, p. 4224, 2019.

[30] V. T. Rathod, "A review of acoustic impedance matching techniques for piezoelectric sensors and transducers," *Sensors*, vol. 20, no. 14, p. 4051, 2020.

[31] E. M. López, "Importancia de la metrología en la determinación del contenido de humedad en granos," *Laboratorio de Humedad en Sólidos, División Termometría, Metrología Eléctrica, Centro Nacional de Metrología: El Marqués, Mexico*, pp. 1–41, 2012.

[32] B. K. Panda, G. Mishra, W. A. Ramirez, H. Jung, C. B. Singh, S.-H. Lee, and I. Lee, "Rancidity and moisture estimation in shelled almond kernels using nir hyperspectral imaging and chemometric analysis," *Journal of Food Engineering*, vol. 318, p. 110889, 2022.

[33] A. Chen, H.-Y. Chen, and C. Chen, "Use of temperature and humidity sensors to determine moisture content of oolong tea," *Sensors*, vol. 14, no. 8, pp. 15593–15609, 2014.

[34] A. d. Santos, R. N. Dean, E. A. Guertal, F. J. O. Morais, P. Carvalhaes-Dias, L. F. C. Duarte, and J. A. S. Dias, "A Reconfigurable Multisensor Based on Printed Circuit Board Technology for Measuring Moisture Content and Temperature in Stored Grain," *IEEE Transactions on Instrumentation and Measurement*, vol. 71, pp. 1–10, 2022.

[35] N. Azmi, L. M. Kamarudin, A. Zakaria, D. L. Ndzi, M. H. F. Rahiman, S. M. M. S. Zakaria, and L. Mohamed, "Rf-based moisture content determination in rice using machine learning techniques," *Sensors*, vol. 21, no. 5, p. 1875, 2021.

[36] R. Wang, F. Han, Y. Jin, and W. Wu, "Correlation between moisture content and machine vision image characteristics of corn kernels," *International Journal of Food Properties*, vol. 23, no. 1, pp. 319–328, 2020.

[37] A. Bhatia, "Principles and Methods of Temperature Measurement,"

[38] J. G. Webster and H. Eren, *Measurement, Instrumentation, and Sensors Handbook: Two-Volume Set*. CRC press, 2018.

[39] P. Viswanadham, *Essentials of Electronic Packaging: A Multidisciplinary Approach*. ASME Press, 2011.

[40] R. S. Khandpur, *Printed circuit boards: design, fabrication, assembly and testing*. New York: McGraw-Hill, 2006. OCLC: ocm62032512.

[41] A. Rivadeneyra and J. A. López-Villanueva, "Recent advances in printed capacitive sensors," *Micromachines*, vol. 11, no. 4, p. 367, 2020.

[42] U. Salmaz, M. A. H. Ahsan, and T. Islam, "High-Precision Capacitive Sensors for Intravenous Fluid Monitoring in Hospitals," *IEEE Transactions on Instrumentation and Measurement*, vol. 70, pp. 1–9, 2021. Conference Name: IEEE Transactions on Instrumentation and Measurement.

[43] L. Fan, Z. Chai, Y. Wang, Z. Wang, P. Zhao, J. Li, Q. Zhou, X. Qin, J. Yao, S. Yan, *et al.*, "A novel handheld device for intact corn ear moisture content measurement," *IEEE Transactions on Instrumentation and Measurement*, vol. 69, no. 11, pp. 9157–9169, 2020.

[44] X. Wang, Y. Wang, H. Leung, S. C. Mukhopadhyay, M. Tian, and J. Zhou, "Mechanism and experiment of planar electrode sensors in water pollutant measurement," *IEEE Transactions on Instrumentation and Measurement*, vol. 64, no. 2, pp. 516–523, 2014.

[45] S. C. Mukhopadhyay, C. P. Gooneratne, G. S. Gupta, and S. N. Demidenko, "A low-cost sensing system for quality monitoring of dairy products," *IEEE Transactions on Instrumentation and Measurement*, vol. 55, no. 4, pp. 1331–1338, 2006.

[46] R. N. Dean, "A PCB Sensor for Detecting Icing Events," *IEEE Sensors Letters*, vol. 5, pp. 1–4, Jan. 2021.

[47] X. Wang, Y. Wang, H. Leung, S. Mukhopadyay, M. Tian, and J. Zhou, "Inorganic Material Detection Based on Electrode Sensor," *IEEE Sensors Journal*, vol. 16, pp. 4147–4148, June 2016. Conference Name: IEEE Sensors Journal.

[48] J. P. d. C. d. Costa, L. C. Junior, E. P. de Araújo, A. d. N. Arantes, E. Longo, A. J. Chiquito, and J. P. Carmo, "Graphite-Based Multianalyte VOC Gas Detection on

Multichannel PCB IDE Sensor," *IEEE Sensors Journal*, vol. 22, pp. 22089–22096, Nov. 2022. Conference Name: IEEE Sensors Journal.

[49] R. F. Corradi, F. Melli, S. Lenzini, N. Cardile, and L. Vincetti, "A Capacitance PCB Sensor for Granular Material With Increased Accuracy," *IEEE Sensors Letters*, vol. 5, pp. 1–4, Oct. 2021. Conference Name: IEEE Sensors Letters.

[50] D. Z. Vasiljevic, G. M. Stojanovic, M. R. Radovanovic, S. Kojic, D. Medic, B. Pivas, and R. Sordan, "PCB sensor for bacteria detection in saline," in *2017 IEEE MTT-S International Microwave Workshop Series on Advanced Materials and Processes for RF and THz Applications (IMWS-AMP)*, pp. 1–3, Sept. 2017.

[51] P. Kassanos, S. Anastasova, and G.-Z. Yang, "A Low-Cost Amperometric Glucose Sensor Based on PCB Technology," in *2018 IEEE SENSORS*, pp. 1–4, Oct. 2018. ISSN: 2168-9229.

[52] R. N. Dean, M. J. Bozack, and R. C. Tighe, "A PCB Sensor for Detecting Ferrous Corrosion Products in Sand," *IEEE Sensors Letters*, vol. 7, pp. 1–4, Feb. 2023.

[53] K. Perveen, G. E. Bridges, S. Bhadra, and D. J. Thomson, "Corrosion Potential Sensor for Remote Monitoring of Civil Structure Based on Printed Circuit Board Sensor," *IEEE Transactions on Instrumentation and Measurement*, vol. 63, pp. 2422–2431, Oct. 2014.

[54] S.-W. Kim, N.-H. Kim, G.-Y. Lee, and G.-S. Kil, "A Sensitivity Comparison of Low-cost Rogowski Coil Sensors for Partial Discharge Measurement of Molded Power Transformers," in *2022 9th International Conference on Condition Monitoring and Diagnosis (CMD)*, pp. 541–544, Nov. 2022. ISSN: 2644-271X.

[55] A. Imburgia, S. Kaziz, P. Romano, D. Flandre, G. Artale, G. Rizzo, F. Viola, F. Tounsi, and G. Ala, "Investigation of PCB-based Inductive Sensors Orientation for Corona Partial Discharge Detection," in *2022 IEEE 21st Mediterranean Electrotechnical Conference (MELECON)*, pp. 559–563, June 2022. ISSN: 2158-8481.

[56] S. Ziegler, R. C. Woodward, H. H.-C. Iu, and L. J. Borle, "Investigation Into Static and Dynamic Performance of the Copper Trace Current Sense Method," *IEEE Sensors Journal*, vol. 9, pp. 782–792, July 2009. Conference Name: IEEE Sensors Journal.

[57] P. N. Kambali and A. K. Pandey, "Nonlinear response of a microbeam under combined direct and fringing field excitation," *Journal of Computational and Nonlinear Dynamics*, vol. 10, no. 5, p. 051010, 2015.

[58] R. N. Dean, A. K. Rane, M. E. Baginski, J. Richard, Z. Hartzog, and D. J. Elton, "A capacitive fringing field sensor design for moisture measurement based on printed

circuit board technology," *IEEE transactions on instrumentation and measurement*, vol. 61, no. 4, pp. 1105–1112, 2011.

[59] R. Marsh, "Selecting thermocouples and platinum resistance temperature detectors," *CONTROL ENGINEERING*, vol. 18, no. 11, p. 76, 1971.

[60] P. Carvalhaes-Dias, I. Ferreira, F. Oliveira Morais, L. Caparroz Duarte, J. Siqueira Dias, and S. Yurish, "Analog linearization of resistance temperature detectors (rtd) using the intrinsic curvature of bandgap voltage references," *Sensors And Electronic Instrumentation Advances (seia'2018)*, pp. 68–71, 2018.

[61] P. Carvalhaes-Dias, I. P. Ferreira, L. F. Duarte, F. J. Morais, and J. S. Dias, "Using the non-linear behavior of the brokaw bandgap voltage reference cell to linearize resistance temperature detectors (rtd)," *Sensors & Transducers*, vol. 229, no. 1, pp. 61–67, 2019.

[62] R. Igreja and C. Dias, "Analytical evaluation of the interdigital electrodes capacitance for a multi-layered structure," *Sensors and Actuators A: Physical*, vol. 112, no. 2-3, pp. 291–301, 2004.

[63] R. Igreja and C. Dias, "Extension to the analytical model of the interdigital electrodes capacitance for a multi-layered structure," *Sensors and Actuators A: Physical*, vol. 172, no. 2, pp. 392–399, 2011.

[64] K. Elangovan and A. C. Sreekantan, "An efficient universal digitizer with linear transfer characteristic for resistive sensor bridges," *IEEE Transactions on Instrumentation and Measurement*, vol. 70, pp. 1–4, 2021.

[65] R. N. Dean, M. A. Reed, and E. A. Guertal, "Optimizing fringing field sensor performance with non-spherical particles," in *2021 IEEE Sensors*, pp. 1–4, IEEE, 2021.

[66] S. O. Nelson, "Measurement and applications of dielectric properties of agricultural products," *IEEE Transactions on Instrumentation and Measurement*, vol. 41, no. 1, pp. 116–122, 1992.

Appendix

APPENDIX A – List of Publication

- **A. d. Santos, R. N. Dean, E. A. Guertal, F. J. O. Morais, P. Carvalhaes-Dias, L. F. C. Duarte, and J. A. S. Dias, "A Reconfigurable Multisensor Based on Printed Circuit Board Technology for Measuring Moisture Content and Temperature in Stored Grain," IEEE Transactions on Instrumentation and Measurement, vol. 71, pp. 1-10, 2022**
- **P. Carvalhaes-Dias, J. Monsalve-Diaz, F. Morais, A. dos Santos, P. Dias-Lima, and J. S. Dias, "Proposal of a reconfigurable sensor for measuring temperature and capacitance," Sensors and Electronic Instrumentation Advances, p. 18, 2020.**
- **A. dos Santos, J. Monsalve-Diaz, P. Carvalhaes-Dias, F. O. Morais, P. Dias-Lima, F. S. Flosi, and J. S. Dias, "Reconfigurable sensor based on pcb technology for moisture and temperature measurement," Sensors & Transducers, vol. 246, no. 7, pp. 1-8, 2020**
- A. D. Dos Santos, S. C. de Brito, A. V. Martins, F. F. Silva, and F. Morais, "Thermoelectric energy harvesting on rotation machines for wireless sensor network in industry 4.0," in 2021 14th IEEE International Conference on Industry Applications (INDUSCON), pp. 694-697, IEEE, 2021.
- F. Morais, P. Carvalhaes-Dias, Y. Zhang, A. Cabot, F. S. Flosi, L. C. Duarte, A. Dos Santos, and J. A. S. Dias, "Low-cost control and measurement circuit for the implementation of single element heat dissipation soil water matric potential sensor based on a snse2 thermosensitive resistor," Sensors, vol. 21, no. 4, p. 1490, 2021
- A. V. Martins, R. M. Bacurau, A. D. dos Santos, and E. C. Ferreira, "Nonintrusive energy meter for nontechnical losses identification," IEEE transactions on instrumentation and measurement, vol. 69, no. 4, pp. 1140-1147, 2019.
- A. D. dos Santos, R. M. Bacurau, A. V. Martins, A. Dante, and E. C. Ferreira, "Simple and low-cost plc modem for iot applications," IEEE Latin America Transactions, vol. 20, no. 12, pp. 2455-2462, 2022.

APPENDIX B – About the author

Adelson dos Santos received the B.E.E. degree in electrical engineering from the University Center of FEI, São Bernardo do Campo, Brazil, in 2015, and the M.S. and Ph.D degrees in electrical engineering from the University of Campinas (UNICAMP), Campinas, Brazil (2018 and 2023). He is currently an associate researcher at Gaugit/IPEN. His current research interests include electronic instrumentation, embedded systems, smart sensors, Internet of Things (IoT), environmental sensors and nuclear instrumentation.